



Department of Precision and Microsystems Engineering

**MODELING OF A REVERBERATION CHAMBER AND ACOUSTIC CONTROL**

SEBASTIAN WEZENBEEK

Report no : 33  
Coach : Dr. Ir. D. de Klerk  
Professor : Prof. Dr. Ir. F. van Keulen  
Specialisation : Engineering mechanics  
Type of report : Master of Science Thesis  
Date : 18-11-2016

Photo: ESA

# ABSTRACT

During a rocket launch a spacecraft is, among other loads, exposed to a potentially damaging acoustic load. Prior to space flight, ground tests are performed to determine whether a spacecraft, or a specific part thereof, can withstand the acoustic load. These tests take place in a reverberation chamber. An acoustic feedback control algorithm shapes the sound field to specified third octave band levels which, are characteristic to individual launch vehicles. When applying feedback control, one faces two challenges. For one, the reverberant room introduces a large time constant resulting in slow transient behaviour, i.e. slow test start-ups. Furthermore amplitude fluctuations are introduced when analysing white noise with third octave band analysis due to its stochastic nature. This causes a lack of precision in steady state operation.

This thesis studies acoustic phenomena taking place in a reverberation chamber. These include non linear sound propagation. The presence and significance of this non linearity will be evaluated. Subsequently, it is aimed to derive an input-output relation, describing the acoustic room response. To extend this relation, the third octave band-pass filters will be studied.

After a physical model is formulated, different feedforward control algorithms are studied to improve both the build-up time of the sound field and the accuracy of the sound field after the steady state is reached. These will first be applied to a single third octave. Thereafter the control system will be extended to multiple third octave bands.



# CONTENTS

<b>1</b>	<b>Introduction</b>	<b>1</b>
1.1	Acoustic testing . . . . .	1
1.2	Goal. . . . .	3
1.3	Thesis outline . . . . .	4
<b>2</b>	<b>Basic principles of acoustics</b>	<b>5</b>
2.1	Sound pressure . . . . .	5
2.2	Addition of sound pressure . . . . .	5
2.3	Sound intensity . . . . .	6
2.4	Sound power . . . . .	6
2.5	Volume velocity . . . . .	6
2.6	Plane wave model versus spherical wave model. . . . .	6
2.7	(Third) octaves . . . . .	8
<b>3</b>	<b>Reverberation chamber acoustics</b>	<b>11</b>
3.1	Modal analysis . . . . .	11
3.1.1	Room modes and resonance frequencies . . . . .	11
3.1.2	Green's function . . . . .	13
3.1.3	Damping. . . . .	15
3.1.4	Multiple receivers . . . . .	20
3.1.5	Modal density . . . . .	20
3.2	The diffuse sound field . . . . .	21
3.2.1	The cut off frequency . . . . .	22
3.2.2	Sound pressure and sound intensity . . . . .	24
3.2.3	Mean free path . . . . .	25
3.2.4	Absorption area . . . . .	25
3.3	Transient acoustic room behaviour . . . . .	26
3.3.1	The diffuse sound field. . . . .	26
3.3.2	The modal approach. . . . .	28
3.4	non linear acoustics. . . . .	28
3.4.1	Adiabatic relations . . . . .	29
3.4.2	The coefficient of non linearity. . . . .	30
3.4.3	non linear propagation . . . . .	31
3.4.4	Propagation after the shock distance. . . . .	33
3.5	non linear acoustics applied on a diffuse field. . . . .	34
3.5.1	Simplified explanation of the simulation. . . . .	34
3.5.2	Extensive explanation of the simulation . . . . .	34
3.5.3	Significance . . . . .	39
3.6	Summary . . . . .	40

<b>4</b>	<b>Modeling</b>	<b>41</b>
4.1	State space representation . . . . .	41
4.2	Identifying <b>A, B, C, and D</b> . . . . .	42
4.2.1	Linear state equations . . . . .	42
4.2.2	Shaped signal to sound power . . . . .	43
4.2.3	Filters . . . . .	43
4.2.4	Model output . . . . .	45
4.3	Transfer function of the model . . . . .	46
4.4	Analysis of the state space model . . . . .	46
4.5	Summary . . . . .	47
<b>5</b>	<b>Control</b>	<b>49</b>
5.1	Control targets . . . . .	50
5.2	Feedforward control . . . . .	51
5.3	Single Input Single Output . . . . .	52
5.3.1	Measurements . . . . .	53
5.3.2	Open loop control . . . . .	53
5.3.3	Feedback control. . . . .	54
5.3.4	Feedforward control: Measuring disturbances. . . . .	55
5.3.5	Feedforward control: Steady state inverse model . . . . .	58
5.3.6	Feedforward control: Elevated initial gains . . . . .	58
5.4	Multiple Input Multiple Output . . . . .	61
5.4.1	Decoupling . . . . .	61
5.4.2	Simulation . . . . .	63
5.5	Summary . . . . .	66
<b>6</b>	<b>Conclusion and future work</b>	<b>69</b>
6.1	Conclusion . . . . .	69
6.2	Future work. . . . .	70
	References . . . . .	71
<b>A</b>	<b>PI vs I in feedback control</b>	<b>73</b>
<b>B</b>	<b>Reverberation times</b>	<b>75</b>

# 1

## INTRODUCTION

During a rocket launch a spacecraft is, among other loads, exposed to a potentially damaging acoustic load. Prior to space flight, ground tests are performed to determine whether a spacecraft, or a specific part thereof, can withstand the acoustic load. These tests take place in a reverberation chamber, typically equipped with large horns for sound generation. See for example figure 1.1.



Figure 1.1: ESA's Large European Acoustic Facility. Photo: ESA

### 1.1. ACOUSTIC TESTING

A sound pressure field is generated within the reverberation chamber to simulate the rocket launch. The acoustic load is huge in terms of energy, i.e. extremely high sound pressure levels are reached. Besides, the sound has a specific spectral pattern. Therefore the desired sound pressure level is specified per third octave frequency band [2]. In figure

1.2 an example of a typical spectral pattern is visualized. The blue line indicates the reference sound pressure level per third octave. The red line indicates the measured sound pressure and the green lines indicate the maximum tolerated deviation. Throughout the test, one aims to generate a sound field with sound pressure levels as close as possible to the reference levels.

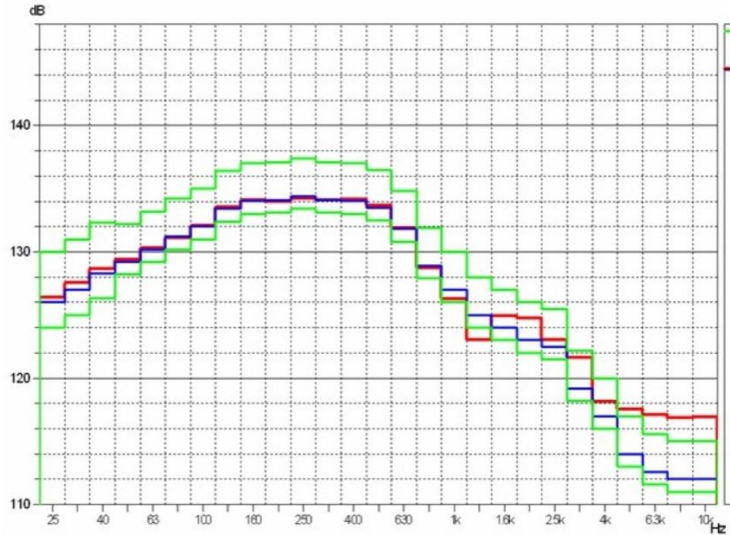


Figure 1.2: Sound pressure levels per third octave bands

A schematic overview of the conventional test facility can be seen in figure 1.3. First Gaussian white noise is generated. Thereafter the white noise is filtered by third octave band pass filters. The resulting signals are then separately amplified, such that the desired spectral pattern is achieved. The signals are then added up, the spectrally shaped signal flows into the acoustic noise generators<sup>1</sup>. In the high reflective room the direct sound field and the powerful reflections form a high energy sound field. The sound pressure in the room is measured by microphones, placed on different locations in the room. The microphone signals are analysed with third octave band filters and thereafter spatially averaged. The sound pressure level per third third octave band is then compared with the reference level. Based on the found error the controller computes new gains.

The controller of this type of testing faces (among other) challenges such as:

1. The control system is a Multi-Input-Multi-Output (MIMO) system, as the sound pressure level has to be controlled in different third-octaves simultaneously. An ideal third octave band filter would attenuate all the frequencies outside its own band. Since ideal filters do not exist in practice, adjacent band pass filters have an overlap in the frequency domain. These overlaps cause interactions between the different third octaves, i.e. exciting only one third octave band, yields output on adjacent third octave bands as well.
2. The sound source generates uncorrelated white noise, which when using third octave band filters, yield a continuous fluctuation of the third octave band ampli-

<sup>1</sup>The noise generators are modulators, they modulate an air or nitrogen flow[1]

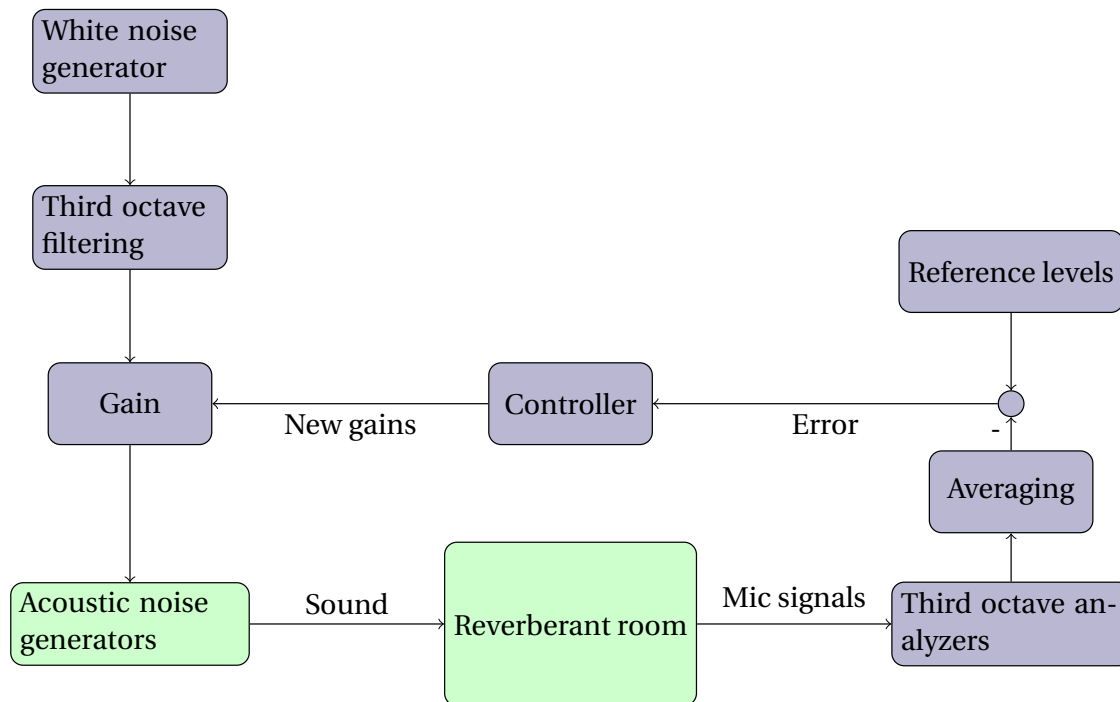


Figure 1.3: Schematic overview of the test

tudes around an average value. In consequence, these fluctuations are also observed in the measurement of the sound pressure field. Feedback controllers can only try and counteract these fluctuations while already happening.

3. The reverberant room introduces a large time constant. The time constant is directly linked to the reverberation time<sup>2</sup>. Reverberation rooms typically have reverberation times well above 10 seconds in practice. Indeed, even when the controller introduces an instant output level increase, it will take time for the sound pressure field to reach a steady state level due to the reverberation room characteristics. Taking into account that overshoot is not allowed in acoustic testing, feedback controllers furthermore do hard on fast transient amplitude steps in the first place. Both phenomena result in long start up times prior to reaching the steady state amplitudes.

## 1.2. GOAL

Taking the control challenges into account, a controller for these tests should be designed. Conventional acoustic control systems use feedback controllers, for instance: [15]. This thesis focuses on applying feedforward control to acoustic testing. The control algorithm is required to improve the performance of the tests in terms of:

1. Rise time
2. Precision & accuracy

<sup>2</sup>The principle of reverberation time will be treated in chapter 3

### 1.3. THESIS OUTLINE

Designing a controller, requires good understanding of the physics taking place. Therefore basic principles of acoustics are introduced in chapter 2. Thereafter acoustical phenomena taking place in a reverberation chamber are discussed in chapter 3. First the sound field is described by the acoustic Eigenmodes in the room. Thereafter the limitations of this approach will be shown and the principle of the diffuse sound field will be introduced. Furthermore the presence of non linear acoustic phenomena is evaluated. Based on the knowledge of the physics learned from chapter 3, a state space representation of the system is derived in chapter 4. Definition of the input-, output- and state variables is determined here. The bandpass filters introduce interactions between the state variables, these are quantified and included in the equations. An identified input-output relation enables decision making for control. In chapter 5 the control problem will first be simplified to a single input single output (SISO) problem. In consequence, different control methods will be designed and evaluated. Their performances is tested in a small reverberation room. Those experimental results are discussed. Thereafter the controller is extended to a MIMO controller. For this purpose a decoupler will be designed. The thesis will be finished with conclusions.

# 2

## BASIC PRINCIPLES OF ACOUSTICS

In order to make this report accessible to those who are not very familiar with acoustics, a short overview of some basic acoustical principles and definitions will be given in this chapter. Basic knowledge of the relations between propagation speed, the wavelength, the wavenumber and frequency is assumed throughout this report. The described relations in this chapter are found in [5], unless stated differently.

### 2.1. SOUND PRESSURE

A graphical representation of a propagating sound wave can be seen in figure 2.1a. It shows the longitudinal behaviour of the wave. Particles move to and fro in the direction of the wave propagation. As a result the medium density and pressure fluctuate around ambient level. The corresponding pressure over distance is represented in figure 2.1b. The sound pressure ( $p$  throughout this report) is defined by the difference between the instantaneous pressure and the atmospheric pressure. To express the sound pressure level, the RMS value over time of this difference is computed. The unit of sound pressure level is therefore Pascal. Though, the sound pressure level is more often expressed as the mean square value in a decibel scale. The reason for this, is that this scale corresponds better with the human experience of sound.

### 2.2. ADDITION OF SOUND PRESSURE

Sound pressure is often caused by multiple sources simultaneously. To compute the collective sound pressure level of different sounds, a careful approach is required. When the frequencies of the different sounds are close to each other, the phase has to be taken into account, the different sound fields interfere in a phase dependent way. When the sounds are incoherent, the square of the total rms pressure can be calculated as follows:

$$p_{\text{total rms}}^2 = \sum_{n=1}^N p_{n \text{ rms}}^2 \quad (2.1)$$

Here  $p_n$  is the sound pressure level corresponding to the  $n$ 'th sound of  $N$  sounds in total.

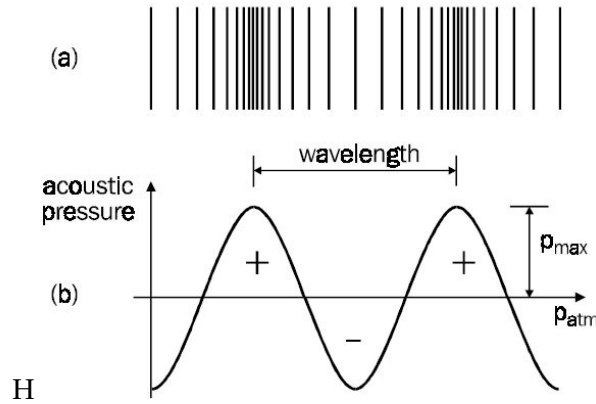


Figure 2.1: Illustration of a wave propagation [7]

### 2.3. SOUND INTENSITY

Sound intensity is a vector quantity. It indicates the amount of power transmitted through a surface normal to the Intensity vector. The magnitude of the sound intensity in a free field can be calculated as follows.

$$I = \frac{p_{\text{rms}}^2}{\rho c_0} \quad (2.2)$$

Here  $p_{\text{rms}}$ ,  $\rho$ , and  $c$  indicate the root mean square of the sound pressure, the density of the medium and the speed of sound respectively. Sound intensity is expressed in decibel.

### 2.4. SOUND POWER

The sound power of a source is the rate of acoustical energy emitted by a sound source. When attenuation losses in the medium are neglected, the sound power can be mathematically defined as the sound intensity normal to an encompassing surface surrounding the source, integrated over this surface:

$$\dot{W} = \int_A \mathbf{I} \cdot \mathbf{n} \, dA \quad (2.3)$$

### 2.5. VOLUME VELOCITY

A source is can also be characterized by its volume velocity  $Q$ . The volume velocity is a flow of air through a surface. In terms of acoustics it is the surface area of the source multiplied by the normal surface particle velocity. When the volume velocity is known, the sound power of the source can be determined:

$$\dot{W} = \frac{\rho \omega^2 Q^2}{8\pi c} \quad (2.4)$$

### 2.6. PLANE WAVE MODEL VERSUS SPHERICAL WAVE MODEL

Throughout this report the sound waves are considered to be plane waves. For now only small perturbations of pressure density and velocity around the steady state are as-

sumed. The linearised conservation of mass, the linearised conservation of momentum and the linearised adiabatic relations can be derived by substituting those small perturbations in the conservation of mass, conservation of momentum and equation of state, while neglecting the higher orders in the perturbations. Furthermore it is assumed that the perturbations are so fast and small that no heat will be transferred.

$$\frac{\partial p}{\partial x} + \rho_0 \nabla \mathbf{u} = 0 \quad (2.5a)$$

$$\rho_0 \frac{\partial \mathbf{u}}{\partial t} = -\nabla p \quad (2.5b)$$

$$p = c_0^2 \rho \quad (2.5c)$$

Those equations can be combined in the linearised plane wave equation [4]..

$$\frac{\partial^2 p}{\partial t^2} = c_0^2 \Delta p \quad \text{with} \quad \Delta p = \frac{\partial^2 p}{\partial x^2} + \frac{\partial^2 p}{\partial y^2} + \frac{\partial^2 p}{\partial z^2} \quad (2.6)$$

The sound pressure for a propagation plane wave can be described by

$$p(x, y, z, t) = \bar{p} e^{i(-k_x x - k_y y - k_z z + \omega t)} \quad (2.7)$$

Here  $\bar{p}$  is an arbitrary amplitude and  $\omega$  represents the radial frequency of the harmonic motion. Substituting equation 2.7 into equation 2.6 yields the relation:

$$\omega^2 = c_0^2 (k_x^2 + k_y^2 + k_z^2) \quad (2.8)$$

In combination with the definition of the wavenumber:

$$k = \frac{\omega}{c_0} \quad (2.9)$$

A constraint can be derived:

$$k^2 = k_x^2 + k_y^2 + k_z^2 \quad (2.10)$$

By integrating the equations of the linearized conservation of momentum [4] over time and distance we can find the relation between the particle velocities  $u$  in the different directions and the sound pressure:

$$\frac{\partial p}{\partial x} + \rho_0 \frac{\partial u_x}{\partial t} = 0 \quad \rightarrow \quad u_x = \frac{k_x}{\omega \rho_0} p \quad (2.11a)$$

$$\frac{\partial p}{\partial y} + \rho_0 \frac{\partial u_y}{\partial t} = 0 \quad \rightarrow \quad u_y = \frac{k_y}{\omega \rho_0} p \quad (2.11b)$$

$$\frac{\partial p}{\partial z} + \rho_0 \frac{\partial u_z}{\partial t} = 0 \quad \rightarrow \quad u_z = \frac{k_z}{\omega \rho_0} p \quad (2.11c)$$

The acoustic impedance  $Z_a$  is the ratio of the sound pressure and the particle velocity. It can be seen that for a plane wave travelling in a single direction the acoustic impedance yields:

$$Z_a = \frac{p}{u} = \rho_0 c_0 \quad (2.12)$$

The impedance for a plane wave in a single direction is also called the characteristic impedance of air  $Z_0$ .

### THE SPHERICAL MODEL

In the spherical model the sound source is treated as a point source. This approach requires the physical dimensions of the sound source to be much smaller than the wavelength of the produced sound. The spherical wave equation is [5]:

$$\frac{\partial^2 p}{\partial r^2} + \frac{2}{r} \frac{\partial p}{\partial r} - \frac{1}{c_0^2} \frac{\partial^2 p}{\partial t^2} = 0 \quad (2.13)$$

Here  $r$  is the distance from the point source. An expression for the sound pressure now is:

$$p(r, t) = \frac{\bar{p}}{r} e^{i(-kr + \omega t)} \quad (2.14)$$

The derivation of the acoustic impedance takes place in an equivalent way as in equations 2.11a and 2.12:

$$u_r = \frac{p}{\rho_0 c_0} \left( 1 - i \frac{c_0}{2\pi f r} \right) \quad (2.15)$$

$$Z_a = \frac{\rho_0 c_0}{1 - i \frac{c_0}{2\pi f r}} \quad (2.16)$$

From eq 2.16 we can conclude that the acoustic impedance for spherical waves approximates the characteristic impedance of air 2.12 when  $2\pi f r \gg c_0$ . Throughout the project this restriction holds. The errors, due to the assumption of plane waves, are mostly insignificant in comparison with the errors accumulated from other assumptions. [5]

## 2.7. (THIRD) OCTAVES

A third octave is a set of frequencies forming a frequency band. The octave scale is defined as follows: The upper band frequency is exactly twice the lower band frequency. Hence, every third octave has twice the bandwidth of its lower adjacent octave. The upper-  $f_u$  and lower band  $f_l$  of a third octave always have the ratio:

$$\frac{f_u}{f_l} = 2^{\frac{1}{3}} \quad (2.17)$$

The frequency bands of some relevant third octaves are defined in table 2.1.

<b>Lower Band Limit (Hz)</b>	<b>Center Frequency (Hz)</b>	<b>Upper Band Limit (Hz)</b>
11.2	12.5	14.1
14.1	16	17.8
17.8	20	22.4
22.4	25	28.2
28.2	31.5	35.5
35.5	40	44.7
44.7	50	56.2
56.2	63	70.8
70.8	80	89.1
89.1	100	112
112	125	141
141	160	178
178	200	224
224	250	282
282	315	355
355	400	447
447	500	562
562	630	708
708	800	891
891	1000	1122

Table 2.1: Frequency limits for third octave bands



# 3

## REVERBERATION CHAMBER ACOUSTICS

In this chapter the Reverberation chamber will be identified. Of interest is the response of the room, i.e. the sound pressure level per frequency band, when the room is excited by a sound source with a certain sound power per frequency band. First a modal analysis will be done. Thereafter the frequency range where the modal analysis is applicable will be determined. Then the diffuse field model will be discussed. finally non linear acoustic phenomena will be identified and quantified.

### 3.1. MODAL ANALYSIS

A reverberation chamber has highly reflective walls. Not much energy is absorbed during a sound wave reflection. As a result, the sound field in the room is a comprises the direct sound field from the source and a lot of its reflections. It is known that a room resonates at certain frequencies. This occurs when for instance a certain amount of wavelengths fits exactly between two walls. The initial wave and its reflections interfere in such a way that a standing wave develops. Those standing waves are called the room modes.

#### 3.1.1. ROOM MODES AND RESONANCE FREQUENCIES

A boundary condition for the chamber is that the fluid or particle velocity normal to the rigid wall is zero at the wall. This boundary condition implies the assumption of zero absorption in the walls. Mathematically this can be stated for the wall in the  $yz$ -plane (figure 3.1).

$$u_x(x = 0, t) = 0 \quad (3.1)$$

Implementing the boundary condition into the linearised momentum equation (equation 2.5b) yields [4]:

$$\rho_0 \frac{\partial u_x}{\partial t} = -\frac{\partial p}{\partial x} \quad \rightarrow \quad \left. \frac{\partial p}{\partial x} \right|_{x=0} = 0 \quad (3.2)$$

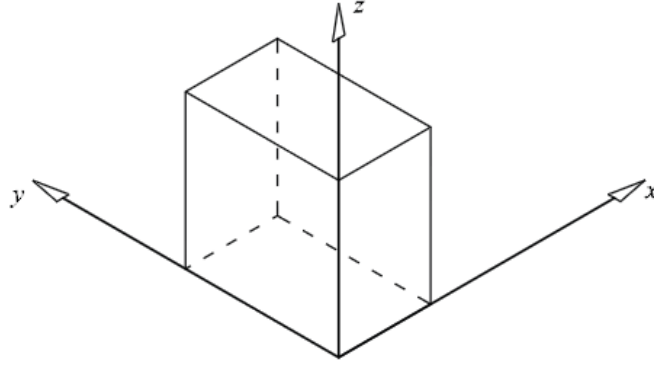


Figure 3.1: Room in coordinate system

This boundary condition can be generalized for the six walls, with the width, length and height of the room being  $l_x$ ,  $l_y$  and  $l_z$ .

$$\left. \frac{\partial p}{\partial x} \right|_{x=0, x=l_x} = 0 \quad \left. \frac{\partial p}{\partial y} \right|_{y=0, y=l_y} = 0 \quad \left. \frac{\partial p}{\partial z} \right|_{z=0, z=l_z} = 0 \quad (3.3)$$

Here it can already be seen that the room modes will be standing waves. In a travelling wave the particle velocity is at its maximum at a pressure peak, whereas here the particle velocity is zero at the peaks.

An harmonic solution for the linear plane wave equation (2.6) is:

$$p(x, y, z, t) = \tilde{p}(x, y, z) \cos \omega t \quad (3.4)$$

Inserting equation 3.4 in equation 2.6 leaves to solve:

$$c_0^2 \left( \frac{\partial^2 \tilde{p}(x, y, z)}{\partial x^2} + \frac{\partial^2 \tilde{p}(x, y, z)}{\partial y^2} + \frac{\partial^2 \tilde{p}(x, y, z)}{\partial z^2} \right) + \omega^2 \tilde{p}(x, y, z) = 0 \quad (3.5)$$

This equation can be seen as an eigenvalue problem. A solution for equation 3.5 which satisfies the boundary conditions at  $x = 0$ ,  $y = 0$  and  $z = 0$  is:

$$\tilde{p}_N(x, y, z) = \bar{P}_N \cos(k_x x) \cos(k_y y) \cos(k_z z) \quad (3.6)$$

Here  $\bar{P}_N$  is amplitude of  $N$ 'th the mode. The magnitude of this amplitude is such that it normalizes the mode. To satisfy the boundary conditions at  $x = l_x$ ,  $y = l_y$  and  $z = l_z$  the following restrictions hold for every positive integer  $n_x$ ,  $n_y$  and  $n_z$ :

$$k_x = \frac{n_x \pi}{l_x} \quad (3.7a)$$

$$k_y = \frac{n_y \pi}{l_y} \quad (3.7b)$$

$$k_z = \frac{n_z \pi}{l_z} \quad (3.7c)$$

Frequency (Hz)	$n_x$	$n_y$	$n_z$
10.46	0	0	1
15.60	0	1	0
18.78	0	1	1
19.06	1	0	0
20.92	0	0	2
21.74	1	0	1
24.63	1	1	0
26.10	0	1	2
26.76	1	1	1
28.31	1	0	2

Table 3.1: Computed first 10 Eigenfrequencies at LEAF

Ideally every sound pressure field can now be described by a combination of modes (shape of the field) and their amplitudes (strength of the field).

$$p(x, y, z, t) = A_N \tilde{p}_N(x, y, z) \cos \omega t \quad (3.8)$$

For every combination of positive integers  $n_x$ ,  $n_y$  and  $n_z$  equation 3.6 gives the spatial shape of the particular Eigenmode of the room. An Eigenmode can be interpreted as a combination of interfering travelling plane waves resulting in a standing wave. There are three types of Eigenmodes. The types are defined by the integers  $n_x$ ,  $n_y$  and  $n_z$ .

- **Axial modes** represent a standing wave parallel to the  $x$ ,  $y$ , or  $z$ -axis. Two of the integers  $n_x$ ,  $n_y$  and  $n_z$  equal zero.
- **Tangential modes** represent a standing wave oblique to two planes of the three planes ( $xy$ ,  $xz$  and  $yz$ ). One of the integers  $n_x$ ,  $n_y$  and  $n_z$  equals zero.
- **Oblique modes** represent a standing wave oblique to all planes. In this situation, all of the integers  $n_x$ ,  $n_y$  and  $n_z$  are non-zero.

The corresponding radial Eigenfrequency or resonance frequency  $\omega_N$  can be determined by equation 2.8. Using the specification of the reverberation room in the Large European Acoustic test Facility (LEAF), the first ten eigenfrequencies of this room can be found (table 3.1) The sound pressure in field in a room can always be described by a combination of all Eigenmodes. One can imagine that for a limited frequency range only a finite amount of modes 'fit' in the room. Furthermore it can be seen that when a ratio between the room dimensions is an integer ( $\frac{l_x}{l_y} = 3$  for instance), different modes will coincide.<sup>1</sup>

### 3.1.2. GREEN'S FUNCTION

The goal is now to describe the sound pressure at a certain point in the room due to a sound source at another location. Since the pressure field is a harmonic function of time,

<sup>1</sup>In this case the the frequency response will be less uniform. therefore a well-designed reverberation chamber does not have dimensions related in such a way. Peaks in the frequency response are not desired, because the frequency response of open air (during a rocket launch) is approximately flat

equation 2.6 can be written as[5]:

$$\Delta p + k^2 p = 0 \quad (3.9)$$

Now a solution for the sound pressure of the sound pressure field at every location  $\mathbf{a}(x, y, z)$  caused by a source located in  $\mathbf{b}(x, y, z)$  with a volume velocity  $Q$  [10].

$$\Delta p(\mathbf{a}, \mathbf{b}) + k^2 p(\mathbf{a}, \mathbf{b}) + i\omega\rho Q\delta(\mathbf{a} - \mathbf{b}) = 0 \quad (3.10)$$

Green's function [6]  $g(\mathbf{a}, \mathbf{b})$  expresses the shape of the sound pressure field caused by a source with a frequency independent volume acceleration. ( $\omega Q = \text{constant}$ )

$$\Delta g(\mathbf{a}, \mathbf{b}) + k^2 g(\mathbf{a}, \mathbf{b}) + \delta(\mathbf{a} - \mathbf{b}) = 0 \quad (3.11)$$

As  $g(\mathbf{a}, \mathbf{b})$  represents a certain sound field it can be expressed by a combination of modes:

$$g(\mathbf{a}, \mathbf{b}) = \sum_{N=1}^{\infty} A_N \tilde{p}_N(\mathbf{a}) \quad (3.12)$$

Equivalently the source term can be expressed by a combination of modes

$$\delta(\mathbf{a} - \mathbf{b}) = \sum_{N=1}^{\infty} B_N \tilde{p}_N(\mathbf{a}) \quad (3.13)$$

It can be shown that Eigenmodes are orthogonal with respect to each other [3]

$$\int_V \tilde{p}_N \tilde{p}_M \, dV = 0 \quad \text{for every } M \neq N \quad (3.14)$$

Whereas,

$$\int_V \tilde{p}_N \tilde{p}_N \, dV = 1 \quad (3.15)$$

Multiplying both sides of equation 3.13 with an arbitrary mode and integrating over the room volume  $V$ , while using the mode properties of equations 3.14 and 3.15 yields:

$$\int_V \delta(\mathbf{a} - \mathbf{b}) \tilde{p}_M(\mathbf{a}) \, dV = \int_V \sum_{N=1}^{\infty} B_N \tilde{p}_N(\mathbf{a}) \tilde{p}_M(\mathbf{a}) \, dV \quad (3.16a)$$

$$\tilde{p}_M(\mathbf{b}) = B_M V \quad (3.16b)$$

$$B_M = \frac{\tilde{p}_M(\mathbf{b})}{V} \quad (3.16c)$$

Equation 3.16c can be substituted into equation 3.13:

$$\delta(\mathbf{a} - \mathbf{b}) = \frac{1}{V} \sum_{N=1}^{\infty} \tilde{p}_N(\mathbf{a}) \tilde{p}_N(\mathbf{b}) \quad (3.17)$$

Now that  $B_N$  is known, an expression for  $A_N$  can be found. Therefore equations 3.12, 3.13 and 3.16c are filled in equation 3.11.

$$\Delta \sum_{N=1}^{\infty} A_N \tilde{p}_N(\mathbf{a}) + k^2 \sum_{N=1}^{\infty} A_N \tilde{p}_N(\mathbf{a}) + \sum_{N=1}^{\infty} \frac{\tilde{p}_M(\mathbf{b})}{V} \tilde{p}_N(\mathbf{a}) = 0 \quad (3.18)$$

Rearrangement gives:

$$(\Delta + k_N^2 - k_N^2 + k^2) \sum_{N=1}^{\infty} A_N \tilde{p}_N(\mathbf{a}) + \sum_{N=1}^{\infty} \frac{\tilde{p}_M(\mathbf{b})}{V} \tilde{p}_N(\mathbf{a}) = 0 \quad (3.19)$$

Here  $k$  is the wavenumber of the harmonic excitation and  $k_N$  is the wavenumber corresponding with the  $N$ 'th eigenfrequency. From equation 3.5 can be concluded that every mode satisfies the linear wave equation:

$$(\Delta + k_N^2) \tilde{p}_N = 0 \quad (3.20)$$

This definition can be used to rewrite equation 3.19:

$$(k^2 - k_N^2) \sum_{N=1}^{\infty} A_N \tilde{p}_N(\mathbf{a}) + \sum_{N=1}^{\infty} \frac{\tilde{p}_M(\mathbf{b})}{V} \tilde{p}_N(\mathbf{a}) = 0 \quad (3.21)$$

Now  $A_N$  can be derived:

$$A_N = - \sum_{N=1}^{\infty} \frac{\tilde{p}_M(\mathbf{b})}{V(k^2 - k_N^2)} \quad (3.22)$$

This expression can be substituted into equation 3.12. Now we can write Green's function as a function of the Eigenmodes.

$$g(\mathbf{a}, \mathbf{b}) = - \sum_{N=1}^{\infty} \frac{\tilde{p}_M(\mathbf{b}) \tilde{p}_M(\mathbf{a})}{V(k^2 - k_N^2)} \quad (3.23)$$

### 3.1.3. DAMPING

Using Green's function the sound pressure field can be determined for a source at a known location with a known volume velocity. Though, Green's function does not yet take the effect of damping in account. As a result the response will be infinite when the the system is excited at a resonance frequency. In this section damping will be added to the function under the assumption that the mode shape does not change due to the damping. Since the damping in a reverberation room is weak, the interfering waves still have approximately the same amplitude and spatial distribution of the undamped field.

#### AIR ATTENUATION

Acoustical energy is absorbed in both the air and the walls of the room. Stokes law of air attenuation states that the amplitude of a sound wave travelling through a medium decreases exponentially with the distance travelled [11] at a rate  $\alpha$ :

$$\alpha_{\text{atn}} = \frac{2\eta\omega^2}{3\rho c^3} \quad (3.24)$$

Here  $\eta$  is the dynamic viscosity of air. The decrease in pressure amplitude over a distance  $x$  can be seen in:

$$p_{\text{peak}}(x) = p_{\text{peak}}(0) e^{-\alpha_{\text{atn}} x} \quad (3.25)$$

The average distance a sound wave travels in the room between two successive reflections, i.e. the 'mean free path' (subsection 3.2.3) is approximately 5 m for the room.

Furthermore, in subsection 3.2.1 will be reasoned that the modal approach can only be used for low frequencies. As  $\rho \gg \eta$  for air and  $c^3 \gg \omega^2$  for the frequency range where a modal analysis can be used,  $\alpha_{\text{atn}}$  will be very small. Therefore, if the decrease in sound pressure due to air attenuation is compared with the decrease in sound pressure due to the wall admittance, we can conclude that the sound energy absorbed by the air, during one free mean path, is negligible compared to the sound energy absorbed by the wall, during a reflection.

## 3

## WALL ADMITTANCE

The specific acoustic impedance is a measure of the opposition to the acoustics flow. It is defined as the ratio between the complex sound particle velocity and the complex sound pressure [5]:

$$Z_a = \frac{p}{u} \quad (3.26)$$

The acoustic surface impedance is the impedance observed by a wave impinging on a surface. When this impedance approaches infinity, the wave will be fully reflected. The rigid wall assumption in the last section implied an infinite impedance at the walls. The acoustic surface impedance represents the dynamics of a surface.

$$Z_{a,n} = \frac{p}{u_n} \quad (3.27)$$

in equation 3.27  $p$  is the complex sound pressure at the surface and  $u_n$  is the component of the complex sound particle velocity, normal to the surface. The specific acoustic wall impedance is obtained by dividing by the characteristic impedance of air (equation 2.12)

$$Z_{a,s} = \frac{Z_{a,n}}{\rho_0 c_0} \quad (3.28)$$

To determine the amount of energy absorbed by the walls, it is convenient to use the inverse of the acoustic surface impedance: the acoustic surface admittance:

$$\beta_{a,s} = \frac{1}{Z_{a,s}} \quad \text{or} \quad \beta_{a,n} = \frac{1}{Z_{a,n}} \quad (3.29)$$

This admittance is a measure for the amount of sound energy that is allowed to flow into the wall. As the local flexibility of the walls is small and the modal analysis is only useful a limited bandwidth (which will be shown in subsection 3.2.1), one can assume that the wall admittance and impedance are real [4]. The phase change is in practice so small that it does not affect the interference pattern. Note that  $\beta_{a,s}$  as well as  $Z_{a,s}$  are dimensionless. Now can be stated that, at the wall, the interface acoustical pressure and the particle velocity, orthogonal to the wall, are related as follows:

$$p = \frac{u_n \rho_0 c_0}{\beta_{a,s}} \quad (3.30)$$

Taking the time derivative and using the linearised momentum equation results in a non-zero left-hand-side of the boundary conditions:

$$\left. \frac{\partial p}{\partial x} \right|_{x=0, x=l_x} = -\beta_{a,n} \rho_0 \frac{\partial p}{\partial t} \quad (3.31)$$

$$\left. \frac{\partial p}{\partial y} \right|_{y=0, y=l_y} = -\beta_{a,n} \rho_0 \frac{\partial p}{\partial t} \quad (3.32)$$

$$\left. \frac{\partial p}{\partial z} \right|_{z=0, z=l_z} = -\beta_{a,n} \rho_0 \frac{\partial p}{\partial t} \quad (3.33)$$

From the boundary conditions we can be concluded that a time variation of the pressure absorbs energy from the system. Hence, the walls act like dampers. With the given boundary conditions taken into account, the harmonic function of equation 3.5 is not a solution to the linear wave equation (2.6) anymore. The solution has to contain a damping term that decays the amplitude exponentially, when the source is turned off:

$$p(x, y, z, t) = \tilde{p}(x, y, z) e^{-\delta t} \cos(\omega t) = \text{Re} (\tilde{p}(x, y, z) e^{i\omega t}) \quad (3.34)$$

Now that damping is added, the resonance frequency  $\underline{\omega}$  is a complex quantity.

$$\underline{\omega} = \omega + i\delta \quad (3.35)$$

To find  $\delta$  it is useful to seek for an expression of the energy in the room. The acoustic energy in a volume consists of a time averaged kinetic and potential part [8].

$$\frac{dE_a}{dV} = \frac{dE_p}{dV} + \frac{dE_k}{dV} = \frac{1}{4\rho_0 c^2} p_{\text{peak}}^2 + \frac{\rho_0}{4} u_{\text{peak}}^2 \quad (3.36)$$

For a mode, i.e a standing wave, the instantaneous energy in a volume only consists of potential energy, when the pressure amplitude reaches its maximum. To visualize this consider the relation of momentum:

$$\rho_0 \frac{\partial u}{\partial t} = -\frac{\partial p}{\partial x} \quad (3.37)$$

When the mode is at its peak pressure in time, the spatial pressure gradient  $\frac{\partial p}{\partial x}$  is at its maximum. From equation 3.37 one can see that the particle acceleration is at its maximum at this moment as well. Since the particle velocity is a harmonic function of time, the particle velocity is zero at this instant. Therefore the instantaneous energy only consist of potential energy:

$$E_{a,N} = \int_V \frac{p_{\text{peak},N}^2}{2\rho c^2} dV = \int_V \frac{A_N^2 \tilde{p}_N^2}{2\rho c^2} dV \quad (3.38)$$

The amount of acoustical energy in the room is the difference between the energy added to and absorbed by the walls. Differentiated in the time domain and applied on a single mode this yields:

$$\dot{W}_{\text{source},N} - \dot{W}_{\text{absorbed},N} = \dot{E}_{a,N} \quad (3.39)$$

When the source is suddenly turned off this becomes:

$$-\dot{W}_{\text{absorbed},N} = \dot{E}_{a,N} \quad (3.40)$$

The rate of energy absorbed is equal to the rate of energy flowing into the walls, i.e. the sound intensity integrated over the total wall surface. Another way of expressing the sound intensity is [5]:

$$I = \frac{\int_0^T p u_n dt}{T} \quad (3.41)$$

Using the relation of equation 3.30 and integrating over the total surface yields:

$$\dot{W}_{\text{absorbed},N} = \int_{S_T} \frac{\int_0^T p_N^2 dt}{T} \frac{1}{\rho_0 c_0} \beta_{a,s} dS_T = \int_{S_T} \frac{A_N^2 \tilde{p}_{,N}^2}{2\rho_0 c_0} \beta_{a,s} dS_T \quad (3.42)$$

Note that the factor 2 in the denominator appears as the pressure in the nominator is described by the mode peak pressure instead of the time averaged pressure (rms). The next step is to find the time derivative of the energy contained in the volume  $\dot{E}_a$ , when a sound field is decaying. I.e. no energy is added by a sound source. Combining the expression of the instantaneous energy (equation 3.38) and the damped solution for the sound pressure field (equation 3.34) yields:

$$E_{a,N} = e^{-2\delta t} \int_V \frac{A_N^2 \tilde{p}_{,N}^2}{2\rho_0 c_0^2} dV \quad (3.43)$$

$$\dot{E}_{a,N} = -2\delta e^{-2\delta t} \int_V \frac{A_N^2 \tilde{p}_{,N}^2}{2\rho_0 c_0^2} dV \quad (3.44)$$

Now consider the moment the source is turned off ( $t=0$ ). Substituting equations 3.42 and 3.44 into equation 3.40 results in an expression for  $\delta$ :

$$\frac{1}{2\rho_0 c_0} \int_{S_T} A_N^2 \tilde{p}_{,N}^2 \beta_{a,s} dS_T = 2\delta \frac{1}{2\rho_0 c_0^2} \int_V A_N^2 \tilde{p}_{,N}^2 dV \quad (3.45)$$

Rearranging,

$$\delta = \frac{c_0}{2} \frac{\int_{S_T} \tilde{p}_{,N}^2 \beta_{a,s} dS_T}{\int_V \tilde{p}_{,N}^2 dV} \quad (3.46)$$

Since the shapes of the modes are not affected by the introduction of damping, equation 3.6 will be used to derive the volume and surface integral. The normalized modes integrated over the total volume equals  $V$  for every mode. The outcome of the surface integral depends on the mode. To generalize an outcome for all axial, tangential and

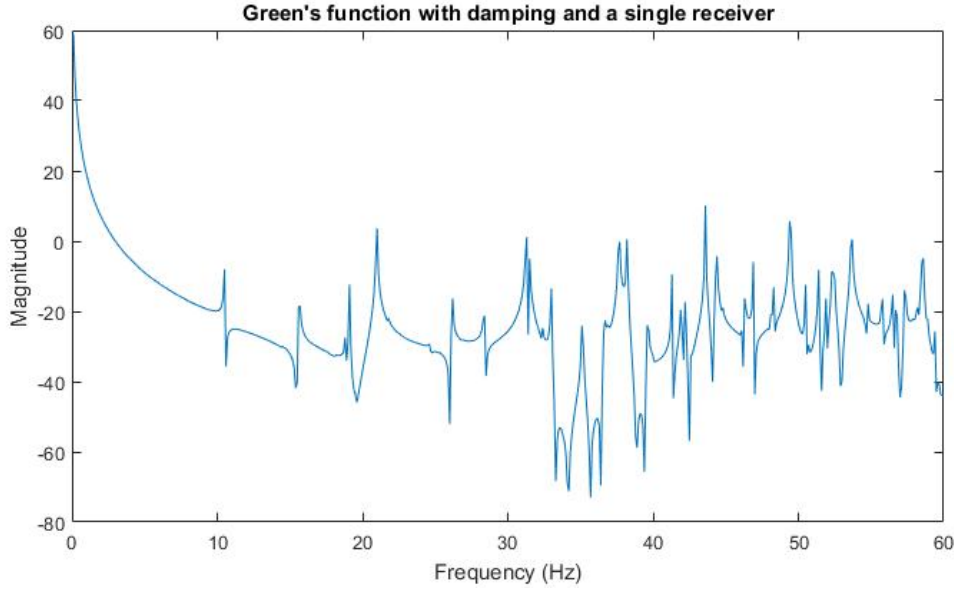


Figure 3.2: Green Function: Single receiver

oblique modes we assume  $l_x \approx l_y \approx l_z$ . While maintaining the total surface area as calculated with the original dimensions. The expressions for  $\delta$  are.

$$\delta_{\text{axial}} = \frac{2}{3V} c_0 S_T \beta_{a,s} \quad (3.47a)$$

$$\delta_{\text{tangential}} = \frac{5}{6V} c_0 S_T \beta_{a,s} \quad (3.47b)$$

$$\delta_{\text{oblique}} = \frac{1}{V} c_0 S_T \beta_{a,s} \quad (3.47c)$$

As can be seen  $\delta_{\text{axial}} < \delta_{\text{tangential}} < \delta_{\text{oblique}}$ . As a result the axial and tangential modes are damped out at a slower rate than the oblique modes. In subsection 3.1.5 will be shown that the oblique modes are more dominant in high frequency bands. Therefore the reverberation time (further explained in subsection 3.3) will be longer in lower frequency bands.

Now that  $\delta$  is known we can implement  $\underline{\omega}$  (equation 3.35) into the Green function (equation 3.23). As the absorption at the walls is small in a reverberation room we neglect the second order damping term ( $\delta^2$ ). The Green function with damping included is:

$$g(\mathbf{a}, \mathbf{b}) = - \sum_{N=1}^{\infty} \frac{\tilde{p}_M(\mathbf{b}) \tilde{p}_M(\mathbf{a})}{V(k^2 - k_N^2 - i k_N \frac{2\delta}{c_0})} \quad (3.48)$$

The damped frequency response of the room up to 100 Hz is shown in figure 3.2. The source is placed at the wall and approximately a meter above the ground. The receiver is placed close to the centre of the room.

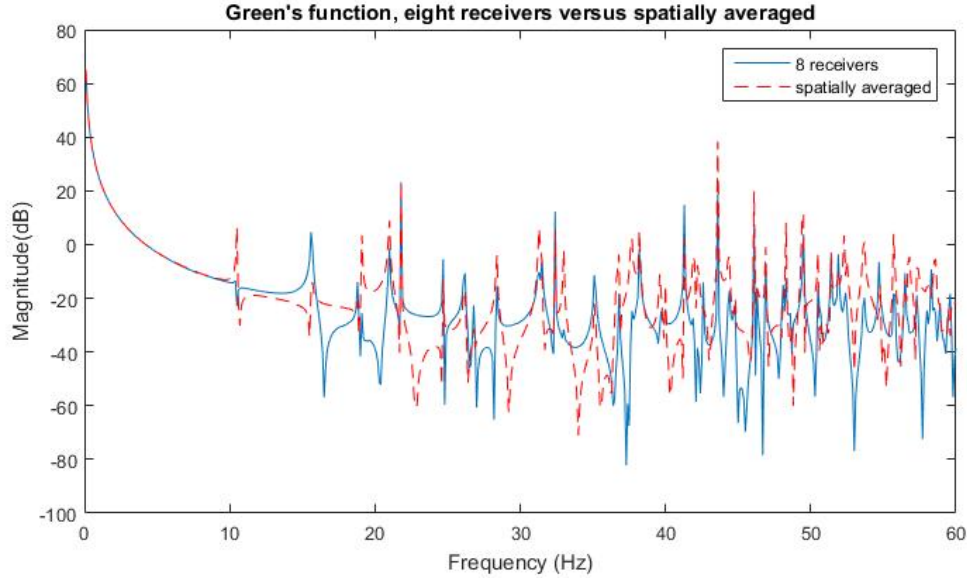


Figure 3.3: Green Function: 8 receivers versus spatially averaged

### 3.1.4. MULTIPLE RECEIVERS

A spatial average gives a better indication how the sound pressure level depends on frequency. A single receiver could be close to nodes of particular modes. In this case, these modes would not be visible in the frequency response. In figure 3.3 the blue line is the averaged frequency response of eight receivers. Compared to figure 3.2 more modes are visible. This indicates indeed a more uniform observability of the different modes. Especially around 35 Hz a clear difference can be observed. Apparently the modes in this frequency range are not strongly observed by the receiver as chosen in figure 3.2.

To determine the frequency response generalized for the complete room, the receiver location dependence is removed from equation 3.48. The source dependence remains, because in practice the source(s) is/are localized on a fixed position:

$$g(\mathbf{b}) = - \sum_{N=1}^{\infty} \frac{\tilde{p}_M(\mathbf{b})}{V(k^2 - k_N^2 - i k_N \frac{2\delta}{c_0})} \quad (3.49)$$

The corresponding frequency response can be seen in figure 3.3. It can be concluded that eight microphones already give an accurate indication of the spatially averaged frequency response.

### 3.1.5. MODAL DENSITY

The modal density is an indication of the number of modes per unit bandwidth. In order to compute the modal density the eigenvalues should be ordered in such a way that the amount of eigenvalues in a certain frequency range can be counted easily. In order to visualize this problem Kuttruff [6] designed a raster in a three dimensional space. In this raster the wavenumbers  $k_N$  or  $k_{n_x, n_y, n_z}$  are located in the raster at location  $(\frac{n_x \pi}{l_x}, \frac{n_y \pi}{l_y}, \frac{n_z \pi}{l_z})$ . Hence every Eigenvalue has its own cube with the volume  $\frac{\pi^3}{l_x l_y l_z} = \frac{\pi^3}{V}$ . The amount

of Eigenvalues in a frequency band up to a certain frequency  $f$  with a corresponding wavenumber  $k$  is equal to the number of eigenvalues contained in a  $\frac{1}{8}$  sphere centered in the origin with radius  $k$ . Consequently, by dividing this volume by the Eigenvalue cube volume, the amount of oblique modes yields:

$$N_{\text{obl}}(k) \approx \frac{k^3 V}{6\pi^2} \quad (3.50)$$

This expression also accounts for 25% of the axial modes and 50% of the tangential modes. The other half of the tangential modes can be determined by:

$$N_{\text{tang, 50\%}} = \frac{\frac{\pi k^2 / 4}{\pi^2 / (l_x l_y + l_x l_z + l_y l_z)}}{2} = \frac{k^2 S_T}{16\pi} \quad \text{with} \quad S_T = 2(l_x l_y + l_x l_z + l_y l_z) \quad (3.51)$$

This amount includes another 50% of the axial modes. The last 25% of the axial modes can be determined by:

$$N_{\text{axial, 25\%}} = \frac{\frac{k}{\pi / (l_x + l_y + l_z)}}{4} = \frac{k l_T}{16\pi} \quad \text{with} \quad l_T = 4(l_x + l_y + l_z) \quad (3.52)$$

The number of modes under a certain frequency  $f$  (corresponding to the wavenumber  $k$ ) yields:

$$N(k) = \frac{k^3 V}{6\pi^2} + \frac{k^2 S_T}{16\pi} + \frac{k l_T}{16\pi} \quad (3.53)$$

From this relation it can be concluded that the amount of oblique modes per unit bandwidth increases at a higher rate than the axial and the tangential modes. Therefore the oblique modes are dominant at higher frequency bands.

To compute the modal density in modes per Herz, We substitute  $k = \frac{2\pi f}{c_0}$  in equation 3.53 and we derive with respect to  $f$ . the modal density yields:

$$n(f) = \frac{dN(f)}{df} = \frac{4\pi f^2 V}{c_0^3} + \frac{\pi f S_T}{2c_0^2} + \frac{L_T}{8c_0} \quad (3.54)$$

### 3.2. THE DIFFUSE SOUND FIELD

Ideally every sound field can be described by the modes derived last section. Though, in practice this is not possible. As can be seen from equation 3.54 the mode density increases rapidly. This can be seen in figure 3.4. When huge amounts of modes are accumulated to represent a sound field, the computation becomes very sensitive to errors. A slight deviation in temperature would for instance affect the speed of sound and therefore the computed sound field would be completely arbitrary. To avoid these problems, from a certain frequency the sound field will be considered to be diffuse. In a diffuse sound field the phase and direction of the sound waves is random. As a result the different sound waves are incoherent and the sound pressure can be added as in equation 2.1. Reverberation chambers are designed to generate a diffuse field, even for low frequencies.

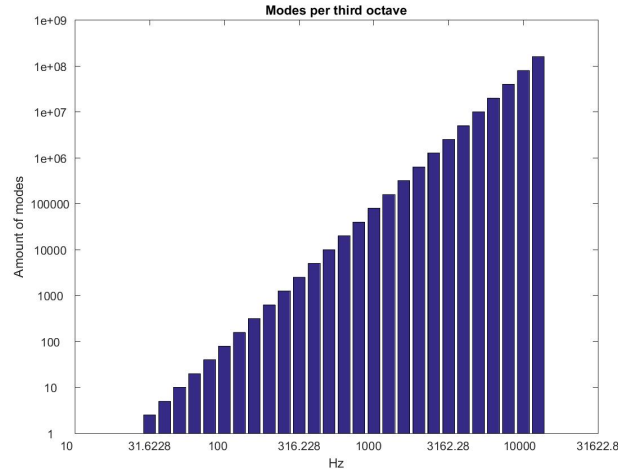


Figure 3.4

### 3.2.1. THE CUT OFF FREQUENCY

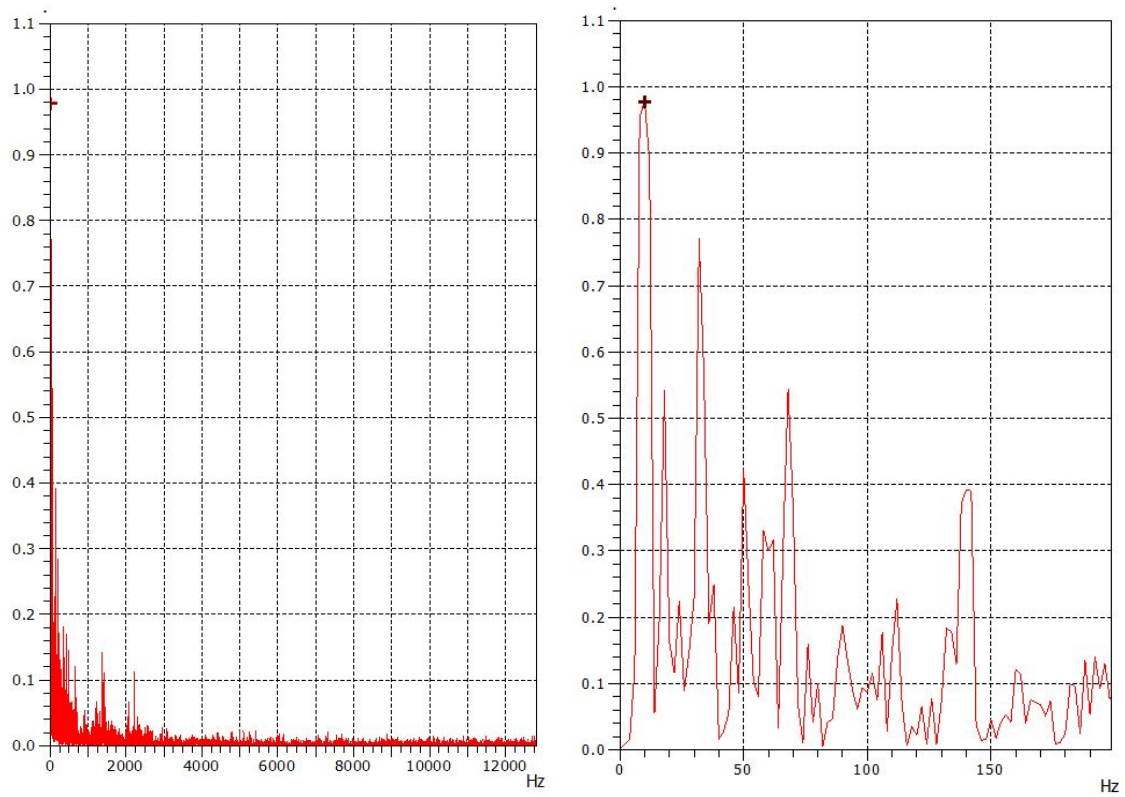
To what extent the different modes overlap is dependent on the modal density and the sound absorption in the room. The modal overlap can be used to determine above which frequency the assumption of a diffuse sound field is justified [3]. Schröder determined that above a certain modal overlap factor a modal analysis loses its strength. The corresponding frequency at which this happens is called the Schröder cut off frequency and can be determined by:

$$f_s = 2000 \sqrt{\frac{T_{60}}{V}} \quad (3.55)$$

Here  $T_{60}$  is the reverberation time, which is described in section 3.3. Experiments show that this frequency is a good estimate for transitioning from the modal analysis into the diffuse sound field approach [12]. Though, blindly using the Schröder cut off frequency has its drawbacks, as it is a generalized relation based on assumptions, plausible if applied in architectural room acoustics, the Schröder frequency for the LEAF room appears to be approximately 210 Hz. In a reverberation chamber, the cut off frequency is expected to be lower than Schröder's frequency, because the room is designed to generate a diffuse sound field. Furthermore the high energy level during a test might amplify the errors introduced by the linear assumptions. Therefore data gathered by a measurement in the LEAF reverberation room in Noordwijk was analysed. The coherence of two signals,  $x$  and  $y$  is defined as [25]:

$$\frac{|G_{xy}(f)|^2}{G_{xx}(f)G_{yy}(f)} \quad (3.56)$$

where  $G_{xy}(f)$  is the Cross-spectral density between  $x$  and  $y$ , and  $G_{xx}(f)$  and  $G_{yy}(f)$  the autospectral density of  $x$  and  $y$  respectively. The coherence of the sound pressure levels measured by two microphones at different locations in the room can be seen in figure 3.5. From this analysis it can be seen that above 150 Hz the coherence is always small. Therefore, in this report the diffuse sound field approach will be applied for the frequency domain above 150 Hz.



(a) A large frequency band

(b) Zoomed in on the cut off area

Figure 3.5: Coherence of two microphone signals

### 3.2.2. SOUND PRESSURE AND SOUND INTENSITY

In a certain frequency band the sound waves have an amplitude  $\bar{p}$ . In a diffuse sound field the waves are incoherent and travelling in every direction. Each plane wave can be described by: (identical to equation 2.7).

$$p(x, y, z, t) = \bar{p}e^{i(-k_x x - k_y y - k_z z + \omega t)} \quad (3.57)$$

The direction of the waves in the three dimensional space can be described by the spherical coordinates  $\theta$  and  $\phi$ :

$$k_x = k \sin \theta \cos \phi \quad (3.58a)$$

$$k_y = k \sin \theta \sin \phi \quad (3.58b)$$

$$k_z = k \cos \theta \quad (3.58c)$$

Taking the squared rms value of a wave in a single direction and integrating in every direction yields the rms value of the sound pressure in the room.

$$p_{\text{rms}}^2 = \frac{\bar{p}^2}{2} \int_0^{2\pi} \int_0^{\pi} \sin \theta d\theta d\phi = 2\pi \bar{p}^2 \quad (3.59)$$

This value is only reliable sufficiently far from the walls. In this project the sound pressure close to the walls is not relevant, as long as it does not affect the sound pressure in the rest of the room. To determine the sound intensity in a certain direction the particle velocity has to be found in this direction. Consider for example the x-direction. Equation 2.11a can alternatively be written:

$$u_x = \frac{k_x}{kc_0\rho_0} p(x, y, z, t) \quad (3.60)$$

Determining the product of the particle velocity and the sound pressure and taking the magnitude yields the sound intensity in x-direction of a wave:

$$I_x = \frac{k_x \bar{p}^2}{2kc_0\rho_0} \quad (3.61)$$

Substituting the relation of equation 3.58a yields the single wave x-direction intensity as a function of  $\theta$  and  $\phi$ . In the perfectly diffuse sound field model the net sound intensity is zero everywhere in the room. The sound intensity incident on a wall can be determined by integrating over a unit hemisphere with radius  $r = \frac{1}{\sqrt{\pi}}$  ( $\pi r^2 = 1$ ).

$$I_{\text{wall},x} = \frac{\bar{p}^2}{2\rho_0 c_0} \int_0^{\pi} \int_0^{\pi} \sin \theta \cos \phi \sin \theta d\theta d\phi = \frac{\pi \bar{p}^2}{4c_0\rho_0} = \frac{p_{\text{rms}}^2}{4c_0\rho_0} \quad (3.62)$$

This relation between the sound intensity per unit area incident to a wall and the rms value of the sound pressure holds for every wall in the room.

### 3.2.3. MEAN FREE PATH

The mean free path is the average distance an arbitrary sound wave travels between two successive reflections. For any enclosed volume the mean free path is [5]:

$$d_{\text{mfp}} = \frac{4V}{S_T} \quad (3.63)$$

To derive this relation the total surface is divided in  $X \rightarrow \infty$  surfaces  $dS_T$ . In each surface a mean free path starts in a particular direction. The surfaces are divided in such a way that the mean free paths are equally divided in space. Now every surface  $dS_T$  is projected on a projection plane perpendicular to the particular mean free path direction. The total projection is called apparent surface area  $S_A$ . The volume of the enclosure equals the product of the mean free path in a single direction  $\bar{d}_{\text{mfp}}$  and the corresponding apparent surface area:

$$V = S_A \bar{d}_{\text{mfp}} \quad (3.64)$$

The mean free path is the average of the mean free path in every single direction  $N$  weighted by the corresponding apparent surface area:

$$d_{\text{mfp}} = \frac{\sum_{N=1}^{\infty} S_{A,N} \bar{d}_{\text{mfp},N}}{\sum_{N=1}^{\infty} S_{A,N}} \quad (3.65)$$

The apparent surface area is:

$$S_A = \frac{1}{2} \int_S |\cos\theta| dS_T \quad (3.66)$$

The apparent surface area averaged over every theta yields:

$$\bar{S}_A = \frac{S_T}{4} \quad (3.67)$$

Substitution of equations 3.67 and 3.64 into equation 3.65 yields equation 3.63.

### 3.2.4. ABSORPTION AREA

The reflection coefficient describes the magnitude and phase change of a wave during a reflection:

$$R = |R|e^{i\gamma} \quad (3.68)$$

In a diffuse sound field the phase of the waves is random. As a consequence the phase change during reflection is irrelevant. Therefore only the magnitude of the reflection coefficient is considered. The absorption coefficient is defined as:

$$\alpha = 1 - |R|^2 \quad (3.69)$$

The reflection and absorption coefficient are dependent on the angle of incidence of the impinging wave. In a diffuse sound field the angle of incidence is random with an equally probability distribution. In this report the absorption coefficient is the statistical absorption coefficient:

$$\alpha = \int_0^{\frac{\pi}{2}} \alpha_{\theta} \sin(2\theta) d\theta \quad (3.70)$$

In subsection 3.1.3 the specific acoustic admittance  $\beta_{a,s}$  was introduced. In a diffuse sound field the absorption coefficient  $\alpha$  is more often used. From the definition of the reflection coefficient it can be shown that  $\alpha$  and  $\beta_{a,s}$  are related [5]:

$$\alpha = 8\beta_{a,s} \quad (3.71)$$

A wall with a surface  $S$  has an absorption area:

$$A_{\text{wall}} = S_{\text{wall}}\alpha \quad (3.72)$$

The absorption area indicates the fraction, of the sound intensity incident to the wall, absorbed by the wall. Not only the walls absorb energy. Objects in the room (the specimen) and air inside the room absorb sound energy as well. Note that air absorption becomes significant as frequency increases. Therefore air absorption cannot be neglected in the high frequency analysis. For the reverberation room the total absorption area roughly yields:

$$A_T = A_{\text{walls}} + A_{\text{specimen}} + A_{\text{air}} \quad (3.73)$$

A total absorption area of 1 m<sup>2</sup> is equivalent to a room with a fully absorbing 1 m<sup>2</sup> wall.

### 3.3. TRANSIENT ACOUSTIC ROOM BEHAVIOUR

The phenomenon of reverberation is well known. The perception of music played by an orchestra in a concert hall is different from the perception in open air. A measure for the amount of reverberation is the reverberation time. When a source in a room is suddenly turned off the sound field in the room decays. The reverberation time  $T_{60}$  is defined as the time required for the sound pressure level to decay 60 decibel.

#### 3.3.1. THE DIFFUSE SOUND FIELD

To derive an expression for the reverberation time the sound pressure as a function of time must be described as a time dependent function  $p(t)$  of the instantaneous sound pressure when the source is turned off  $p(t=0)$

$$p_{\text{rms}}^2(t) = p_{\text{rms}}^2(t=0) (1 - \alpha)^N \quad (3.74)$$

Here  $N$  is the amount of reflections of an arbitrary wave in time  $t$ . By using the mean free path (section 3.2.3)  $N$  can be determined:

$$N = \frac{c_0 t}{d_{\text{mfp}}} \quad (3.75)$$

The time required for the sound pressure level to decay 60 decibel can be obtained by solving:

$$\frac{p_{\text{rms}}^2(t)}{p_{\text{rms}}^2(t=0)} = (1 - \alpha)^N = 10^{-6} \quad (3.76)$$

A solution for  $t$  can be found by using equations 3.75 and 3.63.

$$T_{60} = \frac{-24V \ln 10}{c_0 S_T \ln(1 - \alpha)} \quad (3.77)$$

As  $\alpha \ll 1$  (especially in reverberation rooms) one can assume:  $\alpha \approx \ln(1 - \alpha)$ . As a result the reverberation time can be described by the absorption area  $A_{\text{wall}}$  of the walls. Since not only the walls absorb energy, the reverberation time is a function of the total absorption area  $A_T$ .

$$T_{60} = \frac{-24V \ln 10}{c_0 A_T} \quad (3.78)$$

Measuring the reverberation time is a powerful method to determine the total absorption area of a room. Though, energy absorption is frequency dependent. In consequence the reverberation time only provides information about the absorption in the frequency band it is measured.

### RISE TIME

Transient behaviour does not only appear when a source is turned off. When a source is turned on the sound pressure level needs time to approach the equilibrium sound pressure. The rise time is normally not a subject in acoustics, whereas the reverberation time is one of the most important characteristics in room acoustics. The reason is that the human ear is not as sensitive for sound build up as it is for reverberation. In this project the Rise time is of the essence. The equilibrium sound pressure is reached when the sound power added to the room equals the sound power absorbed by the room:

$$\dot{W}_{\text{source}} = \dot{W}_{\text{absorbed}} \quad (3.79)$$

When the absorption area  $A_T$  is determined by measuring the reverberation time, the absorption power can be determined. The amount of absorbed energy is equal to the energy incident (equation 3.62) on a part of a wall with a surface area  $A_T$ . The equilibrium sound pressure level  $p_{\text{rms,eq}}$  can now be found:

$$\dot{W}_{\text{source}} = \frac{p_{\text{rms,eq}}^2}{4c_0\rho_0} A_T \quad (3.80)$$

The energy density in the room is proportional to the sound pressure. Substituting the particle velocity equations 2.11a, 2.11b and 2.11c in equation 3.36, while remembering the  $k$  number constraint (equation 2.10), yields the acoustical energy density as a function of the rms pressure [9]:

$$\frac{dE_a}{dV} = \frac{p_{\text{rms}}^2}{c_0^2\rho_0} \quad (3.81)$$

In consequence the rate of change of the energy in the room can be described by a differential equation:

$$\frac{d\dot{E}_a}{dV} V = \dot{W}_{\text{source}} - \frac{dE_a}{dV} \frac{c}{4} A_T \quad (3.82)$$

As can be seen the rate of change is the difference between the acoustical energy flowing in and out of the room. The solution for this equation when the source is suddenly turned on is:

$$\frac{dE_a}{dV} = \frac{dE_{a,\text{eq}}}{dV} \left(1 - e^{-\frac{cA_T t}{4V}}\right) \quad (3.83)$$

A general equivalent to the 60 dB reverberation time cannot be found, because this equivalent would be dependent on the strength of the source. Though, a time constant describing the required time to reach a percentage of the equilibrium sound pressure can be found, 90 % for example.

$$T_{90\%} = \frac{-4V \ln 0.1}{c_0 A_T} \quad (3.84)$$

## 3

With other initial conditions the expression for the reverberation time (equation 3.78) can be derived. Furthermore the time response of the room due to a change of sound power can be found by adapting the initial conditions for equation 3.82. The control algorithm will have to take into account that a change in sound power is only sensed after a time delay.

### 3.3.2. THE MODAL APPROACH

The mean square sound pressure level in the room after the source is switched of is already described by equation 3.34.

$$p(x, y, z, t) = \tilde{p}(x, y, z) e^{-\delta t} \cos(\omega t) = \text{Re} (\tilde{p}(x, y, z) e^{i\omega t}) \quad (3.85)$$

Of the essence is that from the definition of  $\delta$  it can be seen that axial modes damp out at a slower rate than tangential and oblique modes. The energy balance can be specified per mode by using equations 3.43 and 3.44:

$$\frac{d\dot{E}_a}{dV_n} = \frac{\dot{W}_{\text{source},n}}{V} - \frac{dE_a}{dV_n} 2\delta_n \quad (3.86)$$

As explained in subsection 3.1.3 axial modes respond slower to changes in sound power than tangential and oblique modes respectively. This is mainly caused by the fact that a propagating wave reflecting between two walls has a longer free path than an oblique wave reflecting between the six room walls. After all most of the energy is absorbed during reflections.

## 3.4. NON LINEAR ACOUSTICS

The linearised plane wave equation (equation 2.6) forms the basis of describing almost every field of acoustics. The linearisation has its limitations, when describing high sound pressure fields. At high sound pressure levels or after long propagation distances non linearities can be observed. There are two main non linear phenomena in acoustics. The first one occurs at extremely high sound pressure levels. As was shown in figure 2.1, a sound wave can be seen as a harmonic pressure fluctuation around the ambient pressure. Now consider the amplitude above and below the ambient pressure separately. The 'above amplitude' is not bounded and can in theory have a value of  $p_0$ . The 'below amplitude', on the other hand, is limited. Its amplitude cannot be higher than  $p_0$ , since the local pressure cannot be lower than zero. Consequently, the pressure profile of a sound wave becomes non symmetric around the ambient pressure line when the sound pres-

sure amplitude approaches the ambient pressure<sup>2</sup>. In a reverberant room the maximum sound pressure level is around 154 dB. At this level the amplitude of sound pressure is only 1.4 % of the ambient pressure (at mean sea level and 20 degrees Celsius). Therefore this non linear phenomenon is not significant and will not be taken into account throughout the report.

The other non linear phenomenon is caused by the fact that high particle velocities propagate faster than low particle velocities. This, in combination with a pressure dependent speed of sound ( $c$  instead of  $c_0$ ) results in distortion of the travelling sound wave. Subsequently higher harmonics will appear in the wave. The significance of this non linear propagation will be evaluated in this section.

### 3.4.1. ADIABATIC RELATIONS

To understand non linear acoustics a part of the derivation of the linear wave equation has to be taken into account. The linear wave equation can be derived when the conservation of mass, the conservation of momentum and the adiabatic relations are combined.

The derivation of the linearised adiabatic relations is taken from Ricksen [4]. Consider a small perturbation of pressure  $p$  and density  $\rho$  around an equilibrium state  $p_0$ ,  $\rho_0$ . Sound propagation in air takes place sufficiently rapidly to assume constant entropy, therefore pressure and density have an adiabatic thermodynamic relation.

$$\frac{p}{\rho^\gamma} = \text{constant} \quad (3.87)$$

Where  $\gamma$  is the ratio of the volume- and pressure specific heat ( $c_v$  and  $c_p$ ) The perturbation can be included in this relation:

$$p_0 + p = \text{constant}(\rho_0 + \rho)^\gamma = \frac{p_0}{\rho_0^\gamma}(\rho_0 + \rho)^\gamma \quad (3.88)$$

The right hand side can be written in a Taylor series expansion:

$$p_0 + p = \frac{p_0}{\rho_0^\gamma}(\rho_0^\gamma + \gamma\rho_0^{\gamma-1}\rho + O(\rho^2)) \quad (3.89)$$

For the linear wave equation the higher order terms are dropped and the relation yields:

$$p = \frac{p_0}{\rho_0^\gamma}(\gamma\rho_0^{\gamma-1}\rho) = \left(\gamma\frac{p_0}{\rho_0}\right)\rho = c_0^2\rho \quad \text{with} \quad c_0^2 = \gamma\frac{p_0}{\rho_0} \quad (3.90)$$

At a sound pressure of 154 dB, acoustics quantities are still small compared to the ambient ones. The Mach number in air at this sound pressure level is:

$$M = \frac{u}{c_0} \approx 0.01 \quad (3.91)$$

<sup>2</sup>A sound pressure level of 191 dB would have peaks of approximately  $p_0$  Sound pressure levels in this order of magnitude are only reached under extreme circumstances (for example: atomic bombs, earthquakes and meteors)

Even though a linear approach can be inaccurate at this sound pressure level, second order equations are sufficient to describe the non linear acousti propagation[13]. A more direct way of writing the equation of state in a Taylor series is:

$$p = \left(\frac{\partial p}{\partial \rho}\right)(\rho) + \frac{1}{2} \left(\frac{\partial^2 p}{\partial \rho^2}\right)(\rho)^2 + \frac{1}{6} \left(\frac{\partial^3 p}{\partial \rho^3}\right)(\rho)^3 \dots \quad (3.92)$$

This can be rewritten to get a linear and quadratic coefficient called:

$$A = \rho_0 \left(\frac{\partial p}{\partial \rho}\right) \quad \text{and} \quad B = \rho_0^2 \left(\frac{\partial^2 p}{\partial \rho^2}\right) \quad (3.93)$$

The ratio between those coefficients is an indication of the non linearity of the medium.

### 3.4.2. THE COEFFICIENT OF NON LINEARITY

In linear acoustics it is assumed that a perturbation of pressure propagates, in the propagation direction  $x$ , with a velocity  $c_0$ .

$$\frac{dx}{dt} = c_0 \quad (3.94)$$

The definition of the speed of sound is based on neglecting the change of entropy [14]:

$$c^2 = \left(\frac{\partial p}{\partial \rho}\right) \quad (3.95)$$

$c_0$  is the linearisation of this function in  $p_0$  and  $\rho_0$ . In reality the perturbation propagation velocity consists of the local speed of sound and the particle velocity:

$$\frac{dx}{dt} = c + u \quad (3.96)$$

$c$  contains the non linearity of the medium. A second order approximation of the non linearity is

$$\frac{dx}{dt} = c_0 + \beta u \quad (3.97)$$

Here  $\beta$  is the coefficient of non linearity, it is related to the constants of  $A$  and  $B$  of equation 3.93 as follows [16]:

$$\beta = 1 + \frac{B}{2A} \quad (3.98)$$

The 1 is present to take the part of the travelling speed, constituted by the particle velocity, into account. The second term represents the second order approximation of the non linearity of the medium. The particle velocity cannot be taken constant at every point in the wave. Using equations 3.87 and 3.93 leads to the expression:

$$\beta = \frac{\gamma + 1}{2} \quad (3.99)$$

### 3.4.3. NON LINEAR PROPAGATION

From the non-linearised conservation of mass and momentum and the equation of state another wave equation (3.101) in terms of the particle velocity can be found for a single direction:

$$\frac{\partial \rho}{\partial t} + u \frac{\partial \rho}{\partial x} + \rho \frac{\partial u}{\partial x} = 0 \quad (3.100a)$$

$$\frac{\partial u}{\partial t} + u \frac{\partial u}{\partial x} + \frac{1}{\rho} \frac{\partial p}{\partial x} = 0 \quad (3.100b)$$

$$p = p(\rho) \quad (\text{Taylor Series}) \quad (3.100c)$$

$$\frac{\partial u}{\partial t} + u \frac{\partial u}{\partial x} + \frac{c^2}{\rho} \frac{\partial \rho}{\partial x} = 0 \quad (3.101)$$

For single direction waves another relation holds [17]:

$$\frac{\partial u}{\partial x} = \frac{c}{\rho} \frac{\partial \rho}{\partial x} \quad (3.102)$$

Combining this relation with equation 3.101 yields:

$$\frac{\partial u}{\partial t} + (u + c) \frac{\partial u}{\partial x} = 0 \quad (3.103)$$

To include the non linearity of the medium, equation 3.97 is substituted in this equation.

$$\frac{\partial u}{\partial t} + (c_0 + \beta u) \frac{\partial u}{\partial x} = 0 \quad (3.104)$$

An implicit solution for this function is:

$$u(x, t) = f(x - (c_0 + \beta u)t) \quad (3.105)$$

The particle velocity of a wave, shortly after generation, can be written as:

$$u(x = 0, t) = u_{\text{peak}} \sin \omega t \quad (3.106)$$

This wave can be taken as an initial condition. With this initial condition, the implicit solution yields:

$$\frac{u}{u_{\text{peak}}} = \sin \left( \omega t - kx \left( 1 + \beta M \frac{u}{u_{\text{peak}}} \right) \right) \quad (3.107)$$

Here the acoustical Mach number appears  $M = \frac{u_a}{c_0}$ . Fubini found a solution, written in an explicit form, using the Bessel functions  $J_n$  [14].

$$\frac{u}{u_{\text{peak}}} = \frac{2}{\beta M k} \sum_{n=1}^{\infty} \frac{J_n(\beta M k n x)}{n x} \sin n(\omega t - kx) \quad (3.108)$$

As can be seen the solution consists of higher harmonics. The amplitude of the harmonics will from now on be called:

$$B_n = \frac{2}{\beta M k n x} J_n(\beta M k n x) \quad (3.109)$$

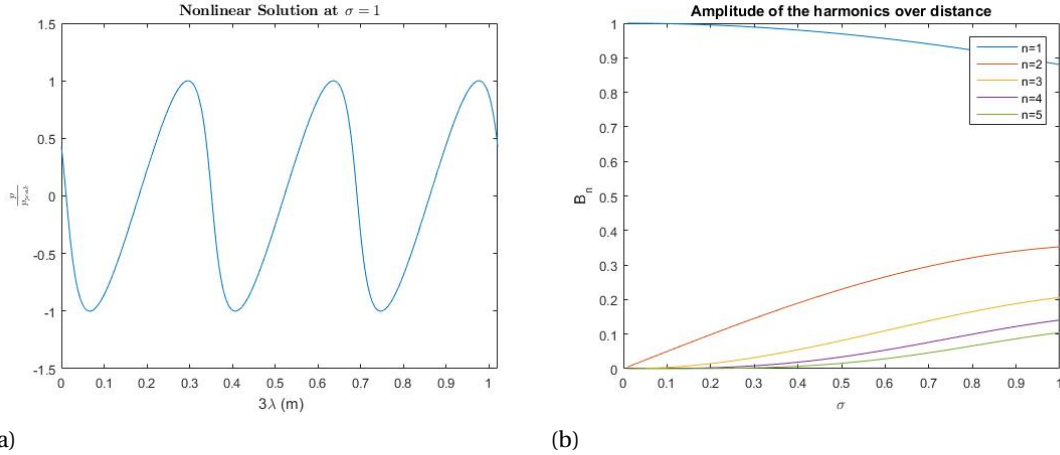


Figure 3.6

The ratio  $\frac{1}{\beta M k}$  is a distance called  $x_{\text{shock}}$ . The solution of equation 3.108 only holds up to this distance. Note that  $x_{\text{shock}}$  is frequency dependent ( $k$ ), as well as sound pressure dependent, since the Mach number is sound pressure dependent. For convenience the dimensionless distance  $\sigma$  is introduced. Which is defined as:

$$\sigma = \frac{x}{x_{\text{shock}}} \quad (3.110)$$

Here  $x$  is the travelled distance of the wave. Using the relation  $p_{\text{peak}} = \rho_0 c_0 u_{\text{peak}}$ <sup>3</sup> equation 3.108 can be rewritten to show the solution for the sound pressure:

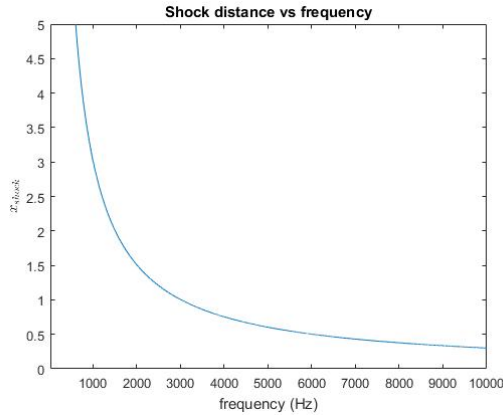
$$\frac{p}{p_{\text{peak}}} = 2 \sum_{n=1}^{\infty} \frac{J_n(n\sigma)}{n\sigma} \sin n(\omega t - kx) \quad (3.111)$$

The sound pressure profile for three wavelengths at the shock distance (i.e.  $\sigma = 1$ ) is shown in figure 3.6a. This solution holds, in theory, for every frequency and sound pressure level. Because the shock distance is frequency and sound pressure dependent.<sup>4</sup> Note that the signal originally was a pure sine wave. It can be seen that after a propagation of  $x_{\text{shock}}$  the signal tends to the shape of a sawtooth wave. The high pressure parts of the wave travel faster, because the particle velocity is positive in these areas. The resulting shape can be described by a sum of higher harmonics (equation 3.111). The growth of the amplitudes of the first five harmonics is shown in figure 3.6b. Note that first the amplitude  $n = 1$  belongs to the frequency of the initial sine wave.

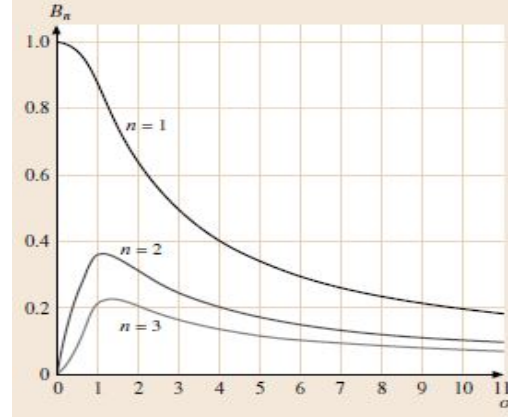
In figure 3.7a the frequency dependence of the shock distance is shown. This graph corresponds to a sound pressure level of 154 dB. As this is the maximum sound pressure

<sup>3</sup>Note that this is a linear approximation of the sound pressure. Though, this approximation is valid, since the sound pressure is still small enough to assume a symmetric pressure profile around the atmospheric pressure.

<sup>4</sup>In practice the shock distance at low sound pressure levels or low frequencies is too long to neglect the decrease of energy density due to divergence. In other words, the accumulated error, caused by describing a spherical wave with a plane wave model, is not acceptable anymore.



(a)



(b) graph taken from [14]

Figure 3.7

level in the reverberation room. As can be seen, in the low frequency range, the shock distance is large in comparison with the mean free path (subsection 3.2.3). As a result the higher harmonics do not get the chance to develop, since relatively much energy is absorbed during a reflection. Therefore the non linear propagation can be ignored in the modal analysis, which is applied in the low frequency range.

#### 3.4.4. PROPAGATION AFTER THE SHOCK DISTANCE

As mentioned, the solution of equation 3.111 is only valid up to a travelled distance of  $x_{\text{shock}}$ . After this distance the losses of energy in the medium cannot be neglected. To properly describe the development of the higher harmonics, one should add a term, describing the thermoviscous losses, to equation 3.104. The resulting equation is the Burger equation [13]:

$$\frac{\partial u}{\partial t} + (c_0 + \beta u) \frac{\partial u}{\partial x} - \frac{1}{2} \delta \frac{\partial^2 u}{\partial x^2} = 0 \quad (3.112)$$

Here  $\delta$ , the diffusivity of sound, is a property of the medium and determines the damping coefficient for a certain frequency:

$$\alpha = \frac{\delta k^2}{2c_0} \quad (3.113)$$

The development of the harmonics can be seen in figure 3.7b. Since energy dissipation is progressively frequency dependent, the development of higher harmonics is small after a travelled distance of  $x_{\text{shock}}$ . Furthermore, the solution of the Burgers equation becomes multivalued after this distance. The resulting change spectral density can not be detected by microphones with the actual sampling rate. Therefore, in this project the non linear propagation of the waves will only be considered up to the shock distance. From there on the propagation will be treated as being linear.

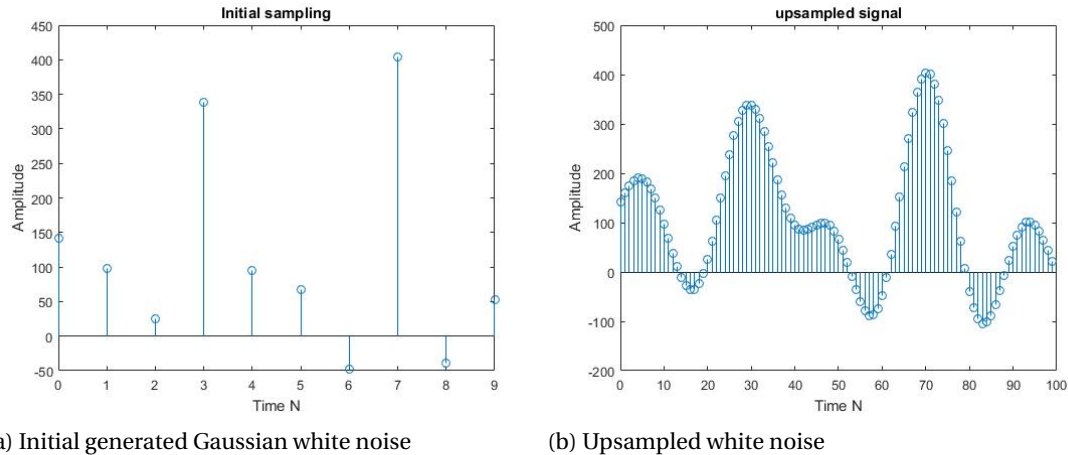


Figure 3.8

### 3.5. NON LINEAR ACOUSTICS APPLIED ON A DIFFUSE FIELD

The interference of non linear sound waves cannot be described by superposition, because the different waves affect each others propagation speed. As a result it is hard to describe the interference of two non linear waves propagating in the same direction algebraically. One can imagine that describing the non linear acoustics in a stochastic diffuse sound field algebraically, is impossible. To encounter this problem, the non linear propagation of sound in a diffuse sound field will be simulated to obtain a quantification of the change in frequency content.

#### 3.5.1. SIMPLIFIED EXPLANATION OF THE SIMULATION

The principle is as follows: A sequence of white noise will be generated and filtered by a third octave filter. In small time steps the non linear propagation of this acoustic noise will be simulated using the second order approximation of the non linear propagation (equation 3.97). The propagation will also be influenced by the interfering diffuse sound field. The particle velocity of the interfering waves will be simulated by adding a stochastic value to the propagation velocity of the noise. After a propagation of approximately the shock distance, the propagated noise will be analysed in the frequency domain and the increase of energy in the high frequency range will be evaluated.

#### 3.5.2. EXTENSIVE EXPLANATION OF THE SIMULATION

As mentioned in subsection 3.2, a diffuse sound field can be described by plane waves in every direction with random phase. In order to find the contribution of the particle velocity to the propagation speed of a perturbation, the particle velocity of the wave, as well as the particle velocity of the interfering waves has to be taken into account.

Assume an overall sound pressure level of  $p_{\text{rms,overall}}$ . The sound pressure in a single point is assumed to be equivalent to the sound pressure at a point uniformly surrounded by sources. These sources produce acoustic Gaussian white noise. According to equation

3.59 the peak pressure of a single sine wave, in a diffuse sound field then yields.

$$\bar{p}^2 = \frac{p_{\text{rms,overall}}^2}{\pi} \quad (3.114)$$

The power  $\bar{P}$  (rms value) of the white noise travelling in a single direction is therefore:

$$\bar{P} = \sqrt{\frac{p_{\text{rms,overall}}^2}{2\pi}} \quad (3.115)$$

A source produces a sequence of Gaussian white noise, with power  $\bar{P}$  in Matlab. The noise is filtered by a third octave filter. For convenience the filtered signal will from now on be referred to as 'the monitored noise'.<sup>5</sup> Initially the monitored noise has a sample frequency of  $f_s = 2^{15}$ . The correlation time of the noise is:  $t_{\text{corr}} = \frac{1}{f_s}$ . Since an interpolation will take place later on, the noise is upsampled with a factor 10. This will increase the accuracy of the numerical approximation. The noise is up sampled by adding zeros between the original samples and then applying an IIR filter [21]. The result can be seen in figure 3.8<sup>6</sup> As the noise represents a sequence of perturbations in pressure, the particle velocity corresponding to the perturbation can be calculated by:

$$u = \frac{p}{c_0 \rho_0} \quad (3.116)$$

The propagation speed of every perturbation is now determined by equation 3.97. In order to visualize and quantify the distortion of the noise, the propagation is simulated. In time steps of  $dt = \frac{1}{2^{15}}$ <sup>7</sup> the propagated distance of every sample is updated. The propagated distance is determined by:

$$dx = \left( c_0 + \beta \frac{p}{c_0 \rho_0} + u_{\text{interf}} \right) dt \quad (3.117)$$

Here  $u_{\text{interf}}$  is the contribution of the diffuse sound field to the propagation speed of the monitored noise. The derivation of this random variable is given in the next subsection.

#### PARTICLE VELOCITY OF THE DIFFUSE SOUND FIELD

In the diffuse field acoustic white noise is travelling in every direction. The acoustical power of the noise travelling in one particular direction, in terms of the overall sound pressure level, is given in equation 3.115. Hence, the sound pressure of noise in one

<sup>5</sup>The name monitored noise is chosen, because the propagation of a sequence of noise through a diffuse sound field will be simulated. The frequency content of this sequence will be 'monitored' to determine the distortion of the noise.

<sup>6</sup>Here, only a small amount of samples is used, for the sake of visibility.

<sup>7</sup>The correlation time of the generated white noise is equal to this time step, as a result  $u_{\text{interf}}$  can be generated as a random value every step. Since the different samples are close to each other in the time domain, the contribution of the diffuse sound field for a certain sample is related to the contribution to its neighbour samples

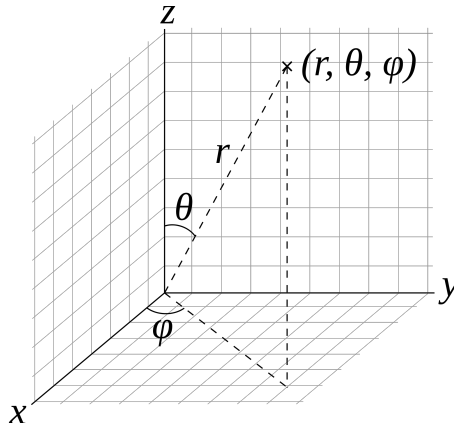


Figure 3.9: Picture taken from *Wikipedia - Spherical coordinate system*

direction  $\bar{p}(\mu, \sigma)$  is a Gaussian distributed quantity with a mean value of zero ( $\mu = 0$ ) and a standard deviation of [19]:

$$\sigma = \sqrt{\bar{P}} \quad (3.118)$$

The definition of  $\theta$  and  $\phi$  can be seen in figure 3.9 (Note that a similar definition is used in section 3.2.2. Though, for another purpose.) Assumed is that the monitored noise is travelling in x-direction.

The particle velocity of noise propagating in an arbitrary single direction  $\bar{u}(\bar{\mu}, \bar{\sigma})$  can be found by using the relation  $u = \frac{p}{c_0 \rho_0}$ . The component of this particle velocity in the direction of the monitored noise (x-direction) can be determined by:

$$\hat{u}(\hat{\mu}, \hat{\sigma}) = \bar{u}(\bar{\mu}, \bar{\sigma}) \sin \theta \cos \phi \quad (3.119)$$

Integrating over a sphere yields the total contribution of the diffuse field to the particle velocity in the x-direction.

$$u_{\text{interf}} = \int_0^{2\pi} \int_0^{\pi} \hat{u}(\hat{\mu}, \hat{\sigma}) \sin \theta d\theta d\phi \quad (3.120)$$

The standard deviation  $\hat{u}(\hat{\mu}, \hat{\sigma})$  is related to the standard deviation of the sound pressure of noise propagating in one direction (equation 3.118)[20]:

$$\hat{\sigma} = \frac{\sin \theta \cos \phi}{c_0 \rho_0} \sigma \quad (3.121)$$

The distribution still has a mean value of  $\hat{\mu} = 0$ .

In the summation normally distributed random variables are added up. Since the mean value is zero, only the addition of the standard deviations has to be considered. When two normal distributions  $A(\mu_A, \sigma_A)$  and  $B(\mu_B, \sigma_B)$  are added up, the standard deviation of the resulting distribution can be determined by [20]:

$$\sigma_{A+B}^2 = \sigma_A^2 + \sigma_B^2 \quad (3.122)$$

To determine the standard deviation of  $u_{\text{interf}}$ , while taking equation 3.122 into account,  $\hat{\sigma}^2$  is integrated over a full sphere.

$$\sigma_{\text{interf}}^2 = \int_0^{2\pi} \int_0^{\pi} \frac{\sin^3 \theta \cos^2 \phi}{c_0^2 \rho_0^2} \sigma^2 d\theta d\phi \quad (3.123)$$

yielding:

$$\sigma_{\text{interf}} = \sqrt{\frac{8\pi}{3}} \frac{\sigma}{c_0 \rho_0} \rightarrow u_{\text{interf}}(0, \sigma_{\text{interf}}) \quad (3.124)$$

Hence,  $u_{\text{interf}}$  is a stochastic value with a normal probability distribution. Since integrating normally distributed random variables might be rather counter intuitive, the double integral is alternatively approximated by setting up the Riemann sum [18]:

$$u_{\text{interf}} = \sum_{j=1}^m \sum_{i=1}^n \hat{u} \left( 0, \frac{\sin \theta_i^* \cos \phi_j^*}{c_0 \rho_0} \sigma \right) \sin \theta_i^* \Delta \theta_i \Delta \phi_j = \sum_{j=1}^m \sum_{i=1}^n \hat{u} \left( 0, \frac{\sin^2 \theta_i^* \cos \phi_j^* \Delta \theta_i \Delta \phi_j}{c_0 \rho_0} \sigma \right) \quad (3.125)$$

Using the relations:

$$\Delta \theta_i = \theta_{i-1} - \theta_i = \frac{\pi}{n} \quad (3.126)$$

$$\Delta \phi_j = \phi_{j-1} - \phi_j = \frac{2\pi}{m} \quad (3.127)$$

$$\theta_i^* = \frac{1}{2}(\theta_i + \theta_{i-1}) \quad (3.128)$$

$$\phi_j^* = \frac{1}{2}(\phi_j + \phi_{j-1}) \quad (3.129)$$

With increasing  $n$  and  $m$  the same result is gathered.

### THE MEASURED SIGNAL

Now that the variables of equation 3.117 are determined, the propagation of the monitored noise will be simulated. For every single sample the travelled distance per time step is accumulated.

$$x = \sum_{i=1}^n dx_i \quad (3.130)$$

Here  $n$  is sufficiently large to assume  $x > x_{\text{meas}}$ .  $x_{\text{meas}}$  is the distance from the source to the receiver. I.e. by choosing the amount of simulation step it is assured every sample will travel past the receiver.

For each sample the travelling time from the source to the receiver is determined.

$$t_{\text{travel}} = i dt + dt_{\text{interp}} \quad (3.131)$$

Since  $x_{\text{meas}}$  is never reached exactly after  $i$  steps,  $dt_{\text{interp}}$  is introduced. It is determined by linear interpolation. The travelling time of each sample is then stored in a vector. From the initial upsampled signal the departure times of the samples are known. Hence,

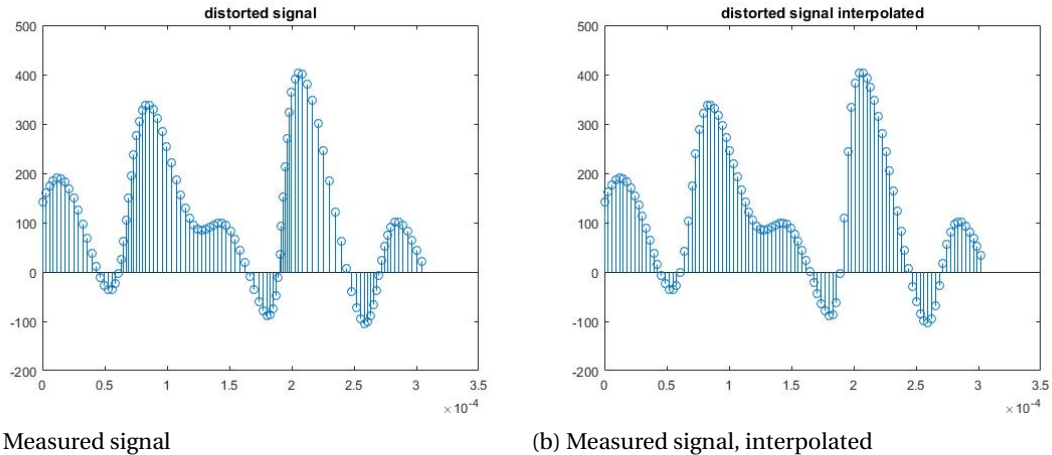


Figure 3.10

the arrival times at the receiver can be determined. These values in combination with the amplitudes of the samples give a discrete received signal with a fluctuating sampling rate. I.e. the samples are not equally spaced in time any more. To determine the frequency content of the signal, the signal will be filtered. Therefore a constant sampling rate is required. This is achieved by a cubic interpolation at points in time according to a fixed sampling rate ( $10f_s$ ). In Matlab the interpolation method called 'pchip' is used, as it uses only four data points to determine the interpolation [21].

The resulting signal can be seen in figure 3.10. It can be seen that the shape of the noise has changed. The left flanks of the positive peaks have steepened, whereas the right sides have flattened. This is a result of the non-linear propagation. The distortion introduces higher harmonics. By filtering the measured signal and analysing the energy change per third octave, the significance of the non-linearities can be quantified.

#### RISETIME AND RINGING

In figure 3.11 a time signal is shown. It is the result of applying the lowest third octave filter on Gaussian white noise. As can be seen in the time signal the bandpass filter needs some time to settle. This phenomenon is taken into account in the simulation. In every signal, only the data after  $t_{\text{rise}}$  is used for the energy calculation.

Due to the sudden change in input, an oscillation in the upsampled signal can be seen at the beginning and end of the signal. This is called ringing. In figure 3.12 the time signal corresponding to the lowest third octave is shown. Zooming in on the end of the dataset shows the unwanted oscillations. To let this phenomenon not affect the energy calculations the first and last 200 samples of the monitored signal is ignored in the energy calculation.

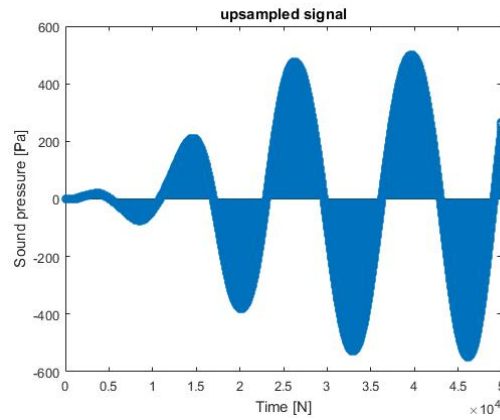
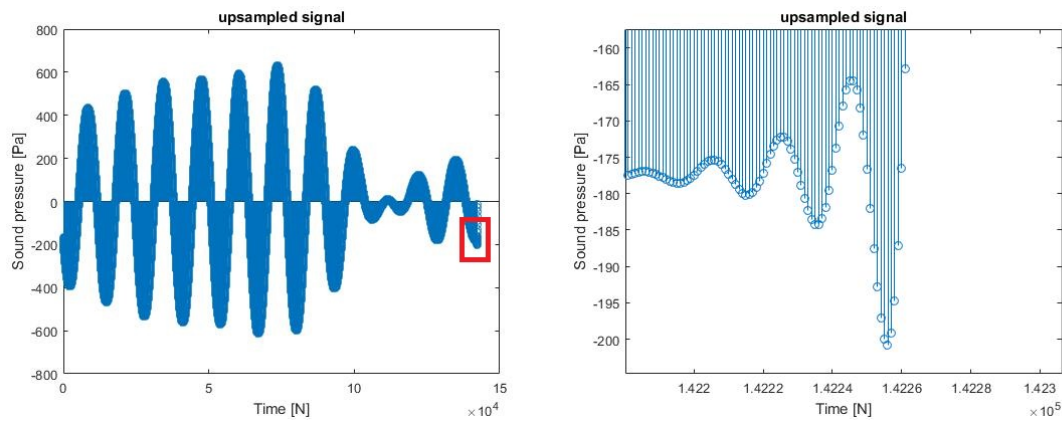


Figure 3.11: Effect of the risetime of a filter



(a) white noise filtered by the lowest third octave band pass filter  
 (b) white noise filtered by the lowest third octave band pass filter. Zoomed in

Figure 3.12: Ringing

### 3.5.3. SIGNIFICANCE

The simulation has been performed multiple times, varying the third octave being excited. However, the general conclusion yields that no significant increase of energy can be observed in other higher third octaves due to non linear sound propagation. Consider for instance the results of table 3.2. Here initially the 1 kHz third octave was excited. In the high third octaves a increase of sound pressure level can be observed. Although 88 dB in the 10 kHz is loud, added to a typical reference level of 115 dB in this third octave it is not significant.  $(115 \text{ dB} + 88 \text{ dB} = 115.008 \text{ dB})$ <sup>8</sup> The biggest absolute increase of sound pressure level can be observed in the 1995 Hz third octave. This is expected, since the first overtones of the 1000 Hz third octave appear in this frequency range. The main conclusion drawn from this simulation is that the non linear propagation does not cause significant leakage of energy into higher third octaves.

<sup>8</sup>In chapter 5 it will be found that a precision of 0.01 dB is not realisable.

Centerfrequency third octave (Hz)	Initial SPL (dB)	Resulting SPL (dB)
1000	141.769099	141.762353
1259	133.952763	133.957141
1585	113.259773	113.238544
1995	100.705792	103.778909
2512	91.7174641	94.6825464
3162	84.0515063	86.2409866
3981	77.6669181	84.8913998
5012	71.1945619	84.8415287
6310	64.9596133	86.5050523
7943	59.0274854	87.0601316
10000	54.5334763	88.0828912

Table 3.2: Simulation results: Excitation of the 1000 Hz third octave

### 3.6. SUMMARY

In this chapter the reverberation room acoustics are identified. First, a modal analysis is performed. The modal approach is only valid in the lower frequency range. The frequency response can be determined by the Green's function. At higher frequencies the modal solution gets too sensitive for small errors. Therefore, above 150 Hz the sound field is assumed to be diffuse. In this model the sound field consists of incoherent sound waves travelling in every direction. This model leads to powerful relations between the sound power of the source and the equilibrium sound pressure level. Furthermore the transient behaviour of the room can easily be described in this way. Describing the acoustics in a linear way might lose accuracy in the higher frequency range. A numerical model is designed in order to quantify the change in frequency content due to non linear acoustical phenomena. From the simulation it can be concluded that the non linear propagation does not cause significant leakage of energy into higher third octaves.

# 4

## MODELING

In this chapter a input-output-relation between the filter gains and the measured sound pressure levels will be derived. The knowledge about the acoustics taking place in the reverberation chamber, learned in chapter 3, will be used to derive this model. Since multiple third octaves have to be controlled, the system has multiple inputs and multiple outputs (MIMO). Therefore the system will be described by a State space model.

### 4.1. STATE SPACE REPRESENTATION

A state space model is a time domain representation of a system [23]. The state model can be written in a vector-matrix form:

$$\dot{\mathbf{x}} = \mathbf{Ax} + \mathbf{Bu} \quad (4.1a)$$

$$\mathbf{y} = \mathbf{Cx} + \mathbf{Du} \quad (4.1b)$$

Since the sound pressure levels of 21 individual third octaves are controlled, the system has 21 states. The number of states is called the order of the system. The state  $\mathbf{x}$  of the system can be described by the mean acoustical energy density, per third octave, in the room. The acoustical energy density in the  $n$ 'th third octave is from now on referred to as<sup>1</sup>:

$$D_n = \frac{dE_{a,n}}{dV} \quad (4.2)$$

The inputs  $\mathbf{u}$  of the system are the squared<sup>2</sup> gains, or amplification factors, computed by the algorithm. The outputs  $\mathbf{y}$  of the system are the computed mean square values of the

---

<sup>1</sup> $D_n$  is not to be confused with  $\mathbf{D}$

<sup>2</sup>The relation between voltage and power is a quadratic relation

measured sound pressure averaged over the different microphones:

$$\dot{\mathbf{x}} = \begin{Bmatrix} \dot{D}_1 \\ \dot{D}_2 \\ \vdots \\ \dot{D}_{21} \end{Bmatrix} \quad \mathbf{x} = \begin{Bmatrix} D_1 \\ D_2 \\ \vdots \\ D_{21} \end{Bmatrix} \quad \mathbf{u} = \begin{Bmatrix} g_1^2 \\ g_2^2 \\ \vdots \\ g_{21}^2 \end{Bmatrix} \quad \mathbf{y} = \begin{Bmatrix} p_{\text{rms},1}^2 \\ p_{\text{rms},2}^2 \\ \vdots \\ p_{\text{rms},21}^2 \end{Bmatrix} \quad (4.3)$$

## 4.2. IDENTIFYING **A**, **B**, **C**, AND **D**

In order to find the entries of **A** and **B** the linear state equations have to be written out. These equations are derived from the relations found in chapter 3.

### 4

### 4.2.1. LINEAR STATE EQUATIONS

As shown in subsection 3.2.1, the sound field can be assumed to be diffuse in the frequency range above 150 Hz. Therefore the state equations for the third octaves 9-21 ( $n = 9 \dots 21$ ) can be derived from the diffuse sound field relations. Equation 3.82 can be rewritten in the form:

$$\dot{D}_n = \frac{\dot{W}_{\text{source},n}}{V} - D_n \frac{cA_{\Gamma,n}}{4V} \quad (4.4)$$

From this equation the relation between  $\dot{\mathbf{x}}$  and  $\mathbf{x}$  ( $\dot{D}_n$  and  $D_n$ ) can be seen. Furthermore this equation contains the sound power of the source  $\dot{W}_{\text{source},n}$ . Note that the transfer function from  $u$  to  $\dot{W}_{\text{source}}$  is not included in the linear state equation yet. This part of the transfer function is determined by filtering and amplification of the signal.

The first eight state equations represent the state of the eight lowest third octaves. In the frequency domain of those third octaves the sound field is not diffuse. In section 3.1 it is shown that Green's function can be used to determine the response in this range. Furthermore the transient behaviour of the sound pressure level is characterized by the parameter  $\delta$ . A relation between the acoustical energy density and the sound power of the source (equivalent to equation 4.4) can be derived from equation 3.42 and 3.39 ( $n = 1, 2, \dots, 8$ ):

$$\dot{E}_{a,n} = \dot{W}_{\text{source},n} - \dot{W}_{\text{absorbed},n} \quad (4.5)$$

$$\dot{D}_n = \frac{\dot{W}_{\text{source},n}}{V} - D_n 2\delta_n \quad (4.6)$$

The value  $\delta_n$  determines the rate of energy dissipation for the  $n$ 'th third octave. Its value depends on the amount of axial, tangential and oblique modes present in the third octave. The decay rate of a mode is characterized in equations 3.46 and 3.47.  $\delta_n$  is defined as:

$$\delta_n = \frac{i_{\text{oblique},n} \delta_{\text{oblique},n} + i_{\text{tangential},n} \delta_{\text{tangential},n} + i_{\text{axial},n} \delta_{\text{axial},n}}{i_n} \quad (4.7)$$

With  $i_n$  indicating the amount of modes in the  $n$ 'th third octave. This formula accounts for the fact that axial modes are less exposed to damping than tangential and oblique

modes. Writing the linear state equations (4.5 and 4.4) in the state space representation (4.1) directly yields the diagonal matrix  $\mathbf{A}$ .

$$\mathbf{A} = \begin{pmatrix} -2\delta_1 & 0 & \cdots & 0 \\ 0 & \ddots & 0 & \\ & 0 & -2\delta_8 & 0 \\ \vdots & & 0 & -\frac{cA_{T,9}}{4V} & 0 \\ & & & 0 & \ddots & 0 \\ 0 & \cdots & & 0 & 0 & -\frac{cA_{T,21}}{4V} \end{pmatrix} \quad (4.8)$$

#### 4.2.2. SHAPED SIGNAL TO SOUND POWER

The matrix  $\mathbf{B}$  does not directly follow from the linear state equations. Because the inputs of the system  $\mathbf{u}$  are not directly included in the state equations. Instead the sound power of the source per third octave  $\dot{W}_{\text{source},n}$  comes up. Therefore a relation between the filter gains and the sound power of the source will be derived. As described in chapter 5, eventually experiments will be performed. These tests will take place in a reverberation room with a amplifier/ loudspeaker combination. Throughout this report a linear relation is assumed between the electrical power dissipated in the noise generators and the sound power they generate.

$$\dot{W}_{\text{source},n} = \eta P_n \quad (4.9)$$

Here  $P_n$  represents the power dissipated in the  $n$ 'th third octave of the signal and  $0 < \eta < 1$  represents the efficiency of converting electrical power into sound power. The relation between the voltage of the amplified and filtered signal and the dissipated power is:

$$P_n = \frac{U_n^2}{R} \quad (4.10)$$

Here  $U$  stands for the rms value of the voltage. Summarizing the preceding formulas: The modulators are modelled as a linear electrical resistance  $R$  where a portion of the energy  $\eta$  is converted into sound energy.

#### 4.2.3. FILTERS

Every third octave band-pass filter in the system is a sixth order Butterworth IIR filter. The magnitude response of the filters are shown in figure 4.1. Note that the frequency axis is scaled logarithmically. From the picture it can be seen that the different filters overlap. This causes interaction in the different octave bands. Actuation of the  $n$ 'th third octave will also affect the  $n + 1$ 'th and the  $n - 1$ 'th third octave.

In figure 4.2a the magnitude response of the 7'th third octave filter is shown. Furthermore the relevant third octave bands are drawn. When white noise is filtered, frequency content belonging to the adjacent third octaves, will also be present in the filtered signal. The purpose is now to quantify the interaction caused by the imperfection of the filters.

Consider the white noise after it has been filtered by the  $n$ 'th third octave filter. The amount of electrical power in the  $m$ 'th third octave of this signal should be determined.

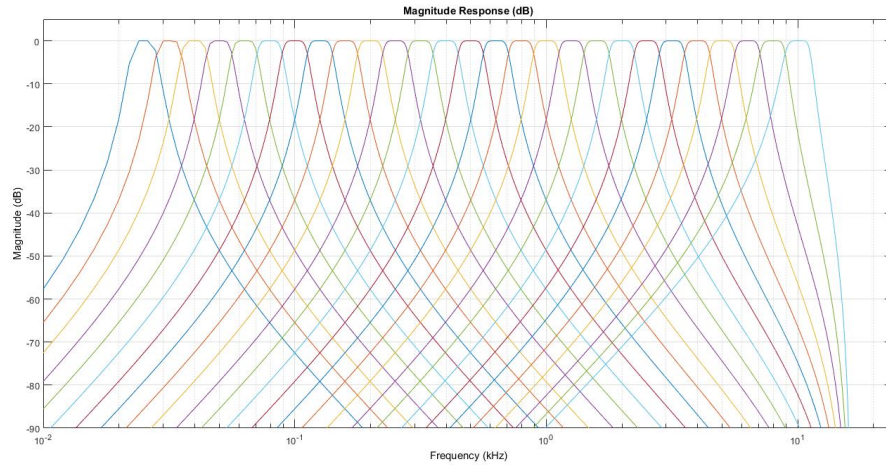
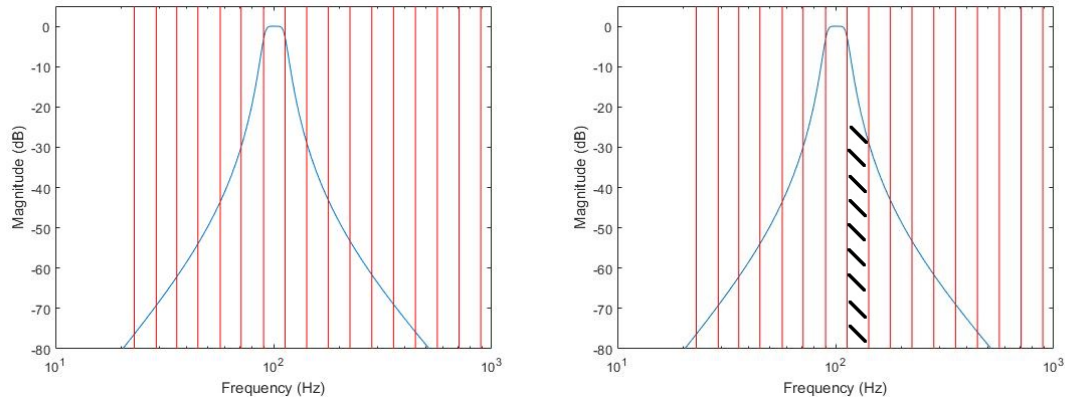


Figure 4.1: Magnitude response of the third octave filters



(a) Magnitude response of the 7th third octave filter (b) Interpretation of  $G_{7,8}$  (center frequency 100 Hz)

Figure 4.2

The white noise has a certain power spectral density  $PSD$ . The definition of white noise is an equal amount of energy in every frequency band  $\Delta f$ . In theory, the signal in every 1 Hz frequency band has an equal rms voltage  $U_{\Delta f=1,wn}$ <sup>3</sup>. After filtering by the  $n$ 'th third octave filter ( $|G_n(f)|$ )<sup>4</sup> and amplification ( $g_n$ ), this value is:

$$U_{n,\Delta f=1}(f) = g_n |G_n(f)| U_{\Delta f=1,wn} \quad (4.11)$$

The rms voltage in a third octave  $m$ , after filtering by the  $n$ 'th third octave filter can be

<sup>3</sup>Note that it is impossible to exactly extract a certain frequency band out of a signal. A filter always has a finite steepness in the frequency domain. Furthermore, this value is stochastic as the white noise is Gaussian in our case.

<sup>4</sup> $|G_n(f)|$  is the filter gain of the  $n$ 'th filter at frequency  $f$

described by summing up every single 1 Hz frequency band in the third octave:

$$U_{mn} = \sqrt{U_{n,\Delta f=1}(f_{m,1})^2 + U_{n,\Delta f=1}(f_{m,2})^2 + \dots + U_{n,\Delta f=1}(f_{m,bw_m})^2} \quad (4.12)$$

Since [26]:

$$RMS_{\text{Total}} = \sqrt{RMS_1^2 + RMS_2^2 + \dots + RMS_n^2} \quad (4.13)$$

Combining and rewriting equations 4.11 and 4.12 gives:

$$U_{mn}^2 = g_n^2 U_{\Delta f=1,wn}^2 (|G_n(f_{m,1})|^2 + |G_n(f_{m,2})|^2 + \dots + |G_n(f_{m,bw_m})|^2) \quad (4.14)$$

For convenience the following notation is defined:

$$G_{mn} = |G_n(f_{m,1})|^2 + |G_n(f_{m,2})|^2 + \dots + |G_n(f_{m,bw_m})|^2 \quad (4.15)$$

$$\mathbf{G} = \begin{Bmatrix} G_{1,1} & \cdots & G_{1,21} \\ \vdots & \ddots & \vdots \\ G_{21,1} & \cdots & G_{21,21} \end{Bmatrix} \quad (4.16)$$

The entry  $G_{mn}$  is a measure for the overlap of the  $n$ 'th filter with the  $m$ 'th third octave. The interpretation of  $G_{8,7}$  can be seen in figure 4.2b. The conclusion of these two subsections can be written down in a formula:

$$\mathbf{w} = \begin{Bmatrix} \dot{W}_{\text{source},1} \\ \dot{W}_{\text{source},2} \\ \vdots \\ \dot{W}_{\text{source},n} \end{Bmatrix} = \frac{\eta U_{\Delta f=1,wn}^2}{R} \mathbf{G} \mathbf{u} \quad (4.17)$$

Substituting equation 4.17 into the linear state equations yields the relation:

$$\dot{\mathbf{x}} = \mathbf{A}\mathbf{x} + \frac{1}{V} \mathbf{w} = \mathbf{A}\mathbf{x} + \underbrace{\frac{\eta U_{\Delta f=1,wn}^2}{RV} \mathbf{G}}_{\mathbf{B}} \mathbf{u} \quad (4.18)$$

Finally  $\mathbf{B}$  can be written:

$$\mathbf{B} = \gamma \mathbf{G} \quad \text{with} \quad \gamma = \frac{\eta U_{\Delta f=1,wn}^2}{RV} \quad (4.19)$$

$\gamma$  is a constant determined by some properties of the plant.

#### 4.2.4. MODEL OUTPUT

The output of the system is defined in equation 4.3. The outputs are the measured mean square sound pressure levels. The sound field is measured by microphones, which are assumed to be linear<sup>5</sup>. The inputs do not have a direct influence on the output<sup>6</sup>. Therefore we can conclude that  $\mathbf{D} = \mathbf{0}$ . The measured mean square sound pressure levels are

<sup>5</sup>The microphone has a constant sound-pressure-to-signal factor over the relevant frequency range

<sup>6</sup>The inputs  $\mathbf{u}$  only influence the output  $\mathbf{y}$  via the state  $\mathbf{x}$ .

not equal to the physical levels, since the signal is again filtered by imperfect third octave filters. The transformation from the sound pressure levels in the room to the measured values is described by  $\mathbf{C}$ .

$$\mathbf{y} = \mathbf{C}\mathbf{x} + \mathbf{D}\mathbf{u} \quad \text{with} \quad \mathbf{D} = \mathbf{0} \quad (4.20)$$

Here  $y_n$  is determined by the amount of energy in the signal filtered by the  $n$ 'th third octave. As has been shown in subsection 4.2.3, part of the energy of adjacent third octaves will pass through the filter. The quantification of this phenomenon is captured in  $\mathbf{G}$ . Though,  $\mathbf{G}$  was designed to compute the energy transfer from a linear power spectrum to an octave power spectrum. The transfer from  $\mathbf{x}$  to  $\mathbf{y}$  is from an octave- to an octave power spectrum. Therefore the rows of  $\mathbf{G}$  have to be normalized, yielding:  $\tilde{\mathbf{G}}$  The relation between the sound pressure levels in the room and the measured ones is:

$$\mathbf{y} = \tilde{\mathbf{G}}^T \mathbf{x} \quad \rightarrow \quad \mathbf{C} = \tilde{\mathbf{G}}^T \quad (4.21)$$

4

### 4.3. TRANSFER FUNCTION OF THE MODEL

The state space model is a useful time domain representation. However, to design a controller, a transfer function matrix in the Laplace domain is more helpful. The transfer function matrix is given by the ratio of the Laplace-transformed output to the Laplace-transformed input:

$$\mathbf{H}(s) = \frac{\mathbf{y}(s)}{\mathbf{u}(s)} \quad (4.22)$$

Laplace transformation of the state space representation ( $\mathbf{D}=\mathbf{0}$ ) yields:

$$s\mathbf{x}(s) = \mathbf{A}\mathbf{x}(s) + \mathbf{B}\mathbf{u}(s) \quad (4.23a)$$

$$\mathbf{y}(s) = \mathbf{C}\mathbf{x}(s) \quad (4.23b)$$

Rearranging of equation 4.23a gives:

$$\mathbf{x}(s) = (s\mathbf{I} - \mathbf{A})^{-1}\mathbf{B}\mathbf{u}(s) \quad (4.24)$$

Substituting this into equation 4.23b results in an input-output relation:

$$\mathbf{y}(s) = \mathbf{C}((s\mathbf{I} - \mathbf{A})^{-1}\mathbf{B})\mathbf{u}(s) \quad (4.25)$$

The transfer function matrix then becomes:

$$\mathbf{H}(s) = \mathbf{C}((s\mathbf{I} - \mathbf{A})^{-1}\mathbf{B}) \quad (4.26)$$

### 4.4. ANALYSIS OF THE STATE SPACE MODEL

From the state space model it is notable that  $\mathbf{A}$  is a diagonal matrix, confirming that no interactions are caused by the acoustics. Nonetheless, the filters do cause interaction between the third octaves. The linear interactions are contained in  $\mathbf{B}$  and  $\mathbf{C}$ . The non diagonal entries of  $\mathbf{H}$  are small in comparison with the diagonal entries. Indicating that the interactions are small. The controllability and observability matrices of equation 4.11

are column full rank and row full rank respectively. Hence, the system is both observable and controllable.

$$C = \begin{Bmatrix} \mathbf{B} \\ \mathbf{AB} \\ \mathbf{A}^2\mathbf{B} \\ \dots \\ \mathbf{A}^{n-1}\mathbf{B} \end{Bmatrix}^T \quad O = \begin{Bmatrix} \mathbf{C} \\ \mathbf{CA} \\ \mathbf{CA}^2 \\ \dots \\ \mathbf{CA}^{n-1} \end{Bmatrix} \quad (4.27)$$

Bringing back the MIMO problem to a SISO problem, i.e. considering only a single third octave, yields the input output relation:

$$H(s) = \frac{y(s)}{u(s)} = \frac{K}{s\tau + 1} \quad \text{with} \quad K = \frac{4\gamma a c_0 \rho_0}{A_{\Gamma}} \quad \text{and} \quad \tau = \frac{4v}{c_0 A_{\Gamma}} \quad (4.28)$$

It can be concluded that the reverberation room is a *first order system*.  $K$  is the steady state gain of the system and  $\tau$  is the time constant. Hence, the SISO system exposes behavior analog to a RC-circuit with a voltage source or a mass damper system with an actuator or an insulated room with a heater. When a constant sound power source is turned on for example, the sound pressure level will build up towards an equilibrium level. One can see the MIMO system as 21 first order systems with small linear interactions.

## 4.5. SUMMARY

The purpose of this chapter is to formulate a state space representation of the system. The inputs are the squared filter gains, the states are the sound pressure levels in the room and the outputs are the measured sound pressure levels. The linear state equations are based on the knowledge gathered in chapter 3. Besides linear behaviour of the acoustic noise generators as well as the microphones is assumed. Furthermore, the filter overlap in the frequency domain is quantified. This quantification determines the non diagonal entries in the transfer function of the system. I.e. the interactions between the third octaves are identified. It is shown that only a single third octave is considered, the system is a first order system. The discoveries from this chapter will be used to choose the control approach in chapter 5.



# 5

## CONTROL

In the previous chapter the transfer function for the system is derived. The purpose of this chapter is to come up with methods to control the plant. As stated in the introduction, conventional feedback control of an acoustic tests faces three main challenges:

1. The control system is a Multi-Input-Multi-Output system, as the sound pressure level has to be controlled in different third-octaves simultaneously. An ideal third octave band filter would attenuate all the frequencies outside its own band. Since ideal filters do not exist in practice, adjacent band pass filters have an overlap in the frequency domain. These overlaps cause interactions between the different third octaves, i.e. exciting only one third octave band, yields output on adjacent third octave bands as well.
2. The sound source generates uncorrelated white noise, which when using third octave band filters, yield a continuous fluctuation of the third octave band amplitudes around an average value. In consequence, these fluctuations are also observed in the measurement of the sound pressure field. Feedback controllers can only try and counteract these fluctuations while already happening.
3. The reverberant room introduces a large time constant. The time constant is directly linked to the reverberation time<sup>1</sup>. Reverberation rooms typically have RT60 times well above 10 seconds in practice. Indeed, even when the controller introduces an instant output level increase, it will take time for the sound pressure field to reach a steady state level due to the reverberation room characteristics. Taking into account that overshoot is not allowed in acoustic testing, feedback controllers furthermore do hard on fast transient amplitude steps in the first place. Both phenomena result in long start up times prior to reaching the steady state amplitudes.

---

<sup>1</sup>The principle of reverberation time will be treated in chapter 3

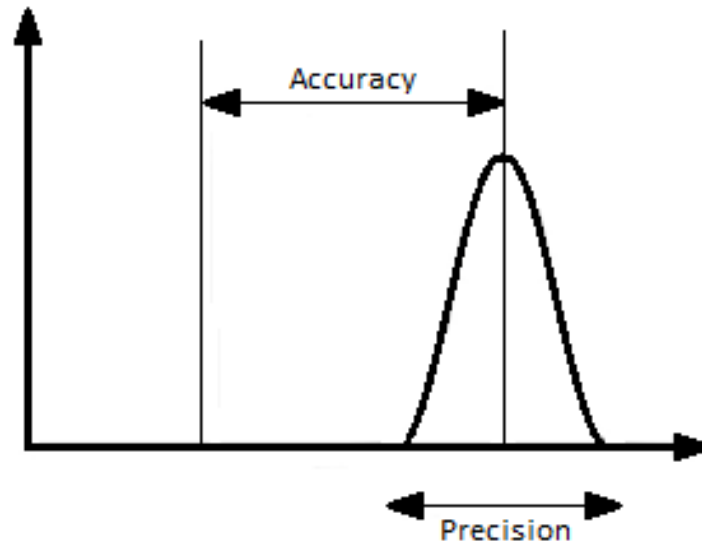


Figure 5.1: Precision versus accuracy

## 5

### 5.1. CONTROL TARGETS

During a test a rocket launch is simulated, the test can only start when the sound pressure level in every third octave is at its reference level. Prior to the test, the sound pressure levels increase towards the reference levels. This start up time can already be a significant acoustic load to which the specimen is exposed. Especially when some of the third octaves already reached their reference level. In this case the specimen is 'overtested'. It is therefore desired that the reference sound pressure levels are reached as fast as possible, minimizing the **rise time**. Though, overshoot of the sound pressure level is strictly not allowed. Overshoot is another, potentially more damaging type of overtesting. Throughout the test, when the reference levels are reached, the sound pressure levels should be as close as possible to the reference levels. Any deviation would cause either over- or under testing. The output has to be both **precise** and **accurate**:

- The measure of precision in this thesis is defined as the maximum absolute deviation from the mean sound pressure level in steady state. Thus in this sense, a good precision implies that the sound pressure level does not vary significantly over time.
- The accuracy is the difference between the mean sound pressure level and the reference level in steady state.

The difference between accuracy and precision is visualized in figure 5.1.

## 5.2. FEEDFORWARD CONTROL

To overcome the mentioned problems of feedback controllers in acoustic testing, the application of feedforward control will be evaluated. Ideally a plant is only influenced by the controller outputs. However, many physical systems have unwanted yet unavoidable other inputs. These inputs are called disturbances. In feedforward control the disturbances are measured and those measurements are taken into account, when the control signal is determined [23]. A block diagram of this working principle is shown in figure 5.3. In this scheme feedforward control is combined with feedback control. The terms and their definitions are summarized in table 5.1.

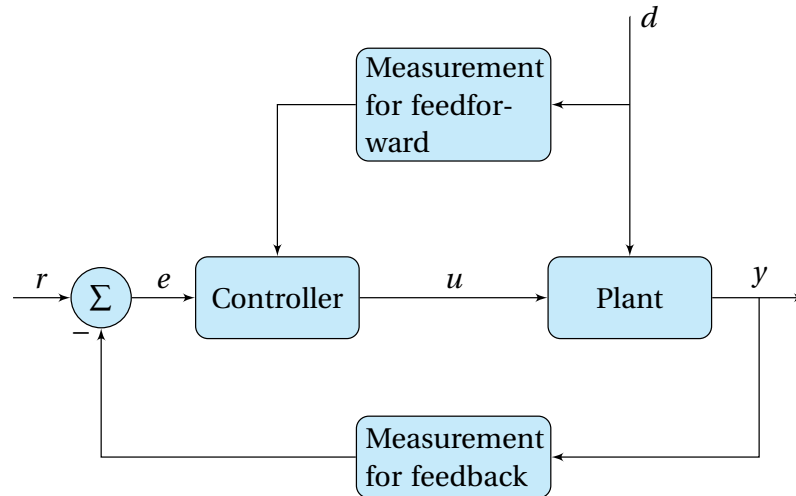


Figure 5.2: Control scheme with both feedback- and feedforward control

Control symbol	Meaning
$r$	Reference signal: reference sound pressure level.
$e$	Control error.
$u$	System input: squared filter gain.
$d$	Disturbances.
$y$	Output: mean square sound pressure level.
Plant	Sound generation and the reverberation room.

Table 5.1: Nomenclature of the control schemes

When a very accurate model of the plant is available, the plant can be controlled without measurement of the output. In this situation one fully relies on the knowledge about the plant, contained in the controller. With this added knowledge, feedforward controllers can easily outperform feedback control when it concerns transient behaviour. Because feedback controllers have to find a the steady state input by trial-and-error, whereas feedforward controllers compute it instantly.

Pure feedforward controllers do not control error-based though, meaning the true system response might be different than computed, potentially yielding inaccurate re-

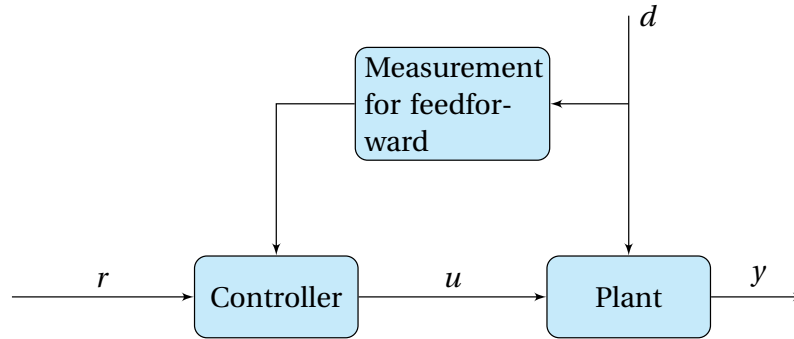


Figure 5.3: Pure feedforward control scheme

sults. It will for our application therefore be researched if feedforward control can serve as a replacement of feedback control or only as an addition to feedback control.

In figure 5.4 an alternative way to generate control signal is shown. This control scheme can be used when the model, derived in chapter 4, appears to be not accurate enough to use for pure feedforward control. Here the feedforward controller typically contains an inverse model of the plant. The benefit is a fast transient behaviour. The input is brought close to its steady state level instantaneously by the feedforward controller. The feedback controller then measures the error (due to the model inaccuracy) and compensates for it.

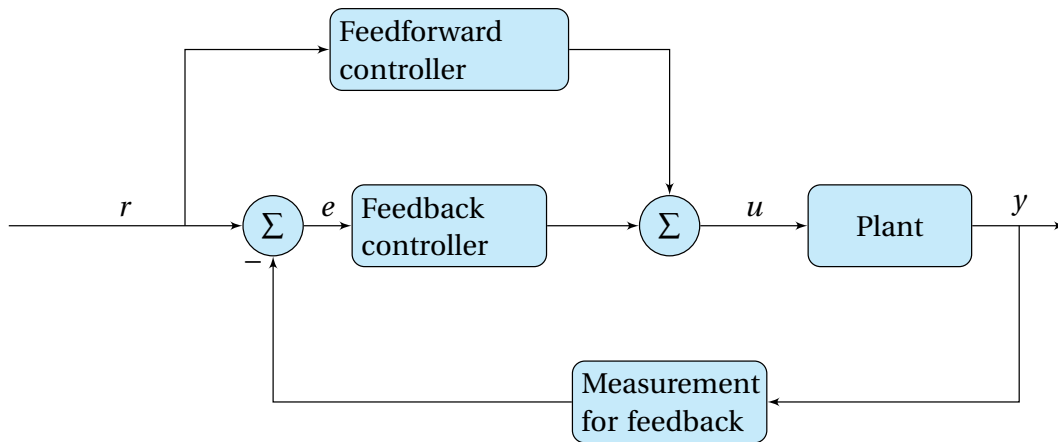


Figure 5.4: Alternative generation of a feedforward control signal

### 5.3. SINGLE INPUT SINGLE OUTPUT

The initial focus is on improving challenge 2 and 3 by the application of feedforward control. Therefore, first only one third octave band is studied. This is done to circumvent octave band interactions as stated in challenge 1, which would possibly falsify this study. In chapter 4 it was found that the SISO transfer function is a first order system:

$$H(s) = \frac{y(s)}{u(s)} = \frac{K}{s\tau + 1} \quad \text{with} \quad K = \frac{4\gamma a c_0 \rho_0}{A_T} \quad \text{and} \quad \tau = \frac{4\nu}{c_0 A_T} \quad (5.1)$$

In this section different control schemes will be designed and thereafter tested.

### 5.3.1. MEASUREMENTS

The different control approaches will be tested in a small reverberation room at MBBM. The properties of the room are listed in table 5.2.

Property	Value
Volume V (m <sup>3</sup> )	200
Absorption area A at 1000 Hz (m <sup>2</sup> )	6.3
Reverberation time T60 at 1000 Hz (s)	5.11
Diffuse frequency domain (Hz)	> 100 Hz
Amount of microphones	3

Table 5.2: Nomenclature of the control schemes

The acoustic noise generators are linear loudspeakers. The control algorithms operate in Simulink® Real-Time™ and communicate with the loudspeakers and microphones via a sound card. First the microphone signals are analysed separately and thereafter added. The controlled third octave band has a centre frequency of 1000 Hz. The reference level for this test will be 92 dB.

### 5.3.2. OPEN LOOP CONTROL

This subsection describes the modelling and testing of the open loop scheme shown in figure 5.5. As stated in section 5.2, a pure feedforward controller requires a very accurate model. By testing the open loop controller, the accuracy of the physical model (equation 5.1) is tested. Furthermore, open loop control will give a first indication how significantly disturbances affect the output.

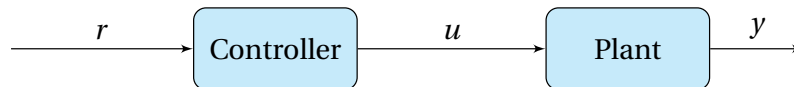


Figure 5.5: Open loop control scheme

Since the reverberation room is a first order system, a prediction on its response can easily be made. From equation 5.1 it can be derived that the steady state gain of the system ( $s \rightarrow 0$ ) is  $K$ . Therefore the steady state output of the system will be  $y = Ku$ . With the controller gain in steady state  $C_{ss}$ , the transfer function from reference to output in steady state can be derived:

$$Y_{ss} = rC_{ss}K \quad (5.2)$$

In order to let the output of the system match with the reference level in steady state the controller should have a transfer function of:

$$C = K^{-1} \quad (5.3)$$

## RESULTS

As can be seen in figure 5.6 the sound pressure level moves towards the reference level quickly. After reaching steady state an error of approximately -1 dB remains though. One can therefore conclude that the model is not accurate enough. The open loop controller furthermore has a precision of 1.2 dB.

One might think that a slight adjustment to the transfer function amplitude would be sufficient to compensate for the error. Though, it was found that the room response can differ from test to test, the open loop control model does not take that into account.

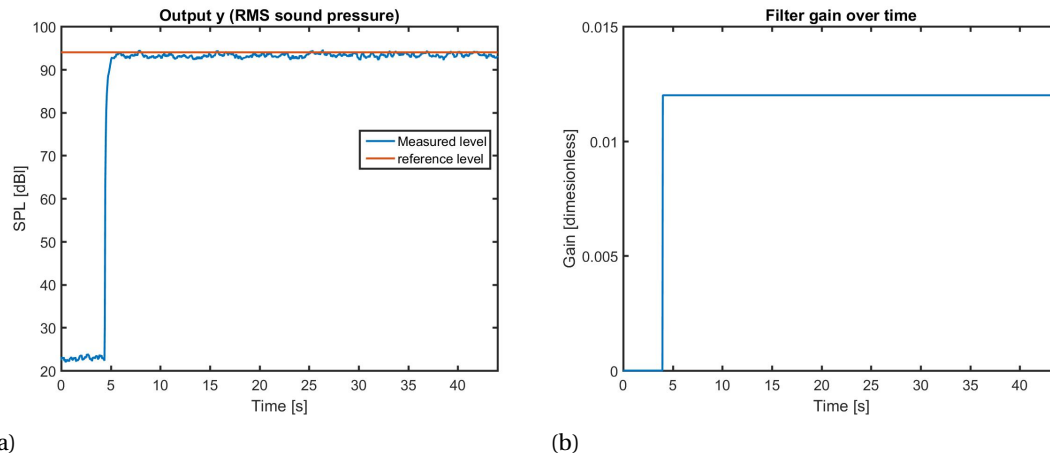


Figure 5.6: Performance of the open loop control

### 5.3.3. FEEDBACK CONTROL

Since the model of the plant is shown to be not accurate enough for open loop control, feedback control is required to eliminate the steady state error of 1 dB. Therefore a conventional feedback controller is designed. The control scheme can be seen in figure 5.7. The controller is a PI controller. A derivative action is omitted as it accounts for future values of the error. As a result it is sensitive for noise signals. The controller is first tuned using the Ziegler-Nichols method. Thereafter it is further manually tuned such that overshoot is prevented.

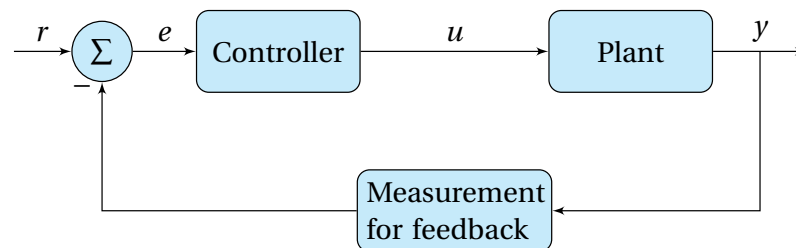


Figure 5.7: Feedback control scheme

## RESULTS

In comparison with the open loop control, the steady state error has disappeared (see figure 5.8). Since the controller is tuned to both prevent overshoot and not overreact on small perturbations, it needs some time to settle. In terms of precision the feedback control is not superior to the open loop control. The precision is about 1.1 dB, e.g. in steady state, the controller output has a considerable variance. The controller tries to compensate for the fluctuations in the sound signal, but seems to lack speed. As will be shown in subsection 5.3.4, a large portion of this fluctuation is due to the way the sound pressure field is excited and evaluated: usage of third octave band filters on true random noise.

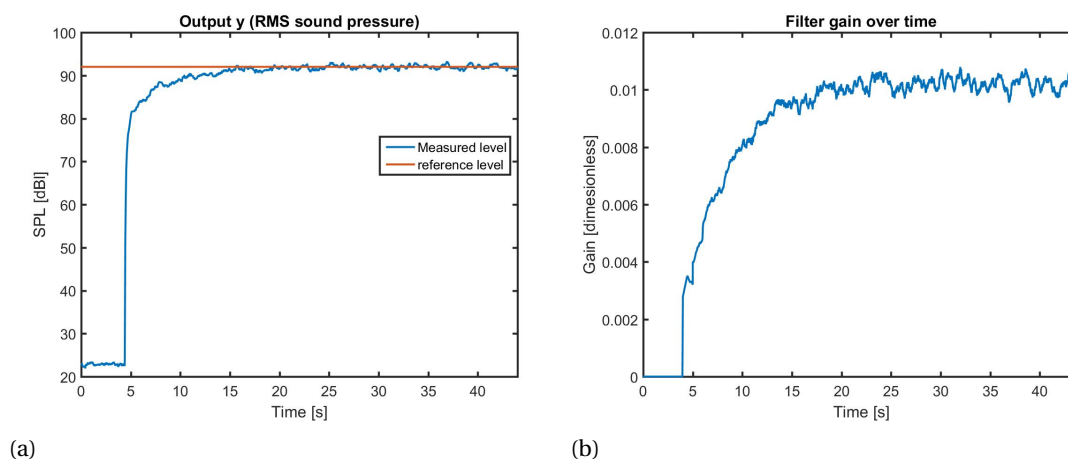


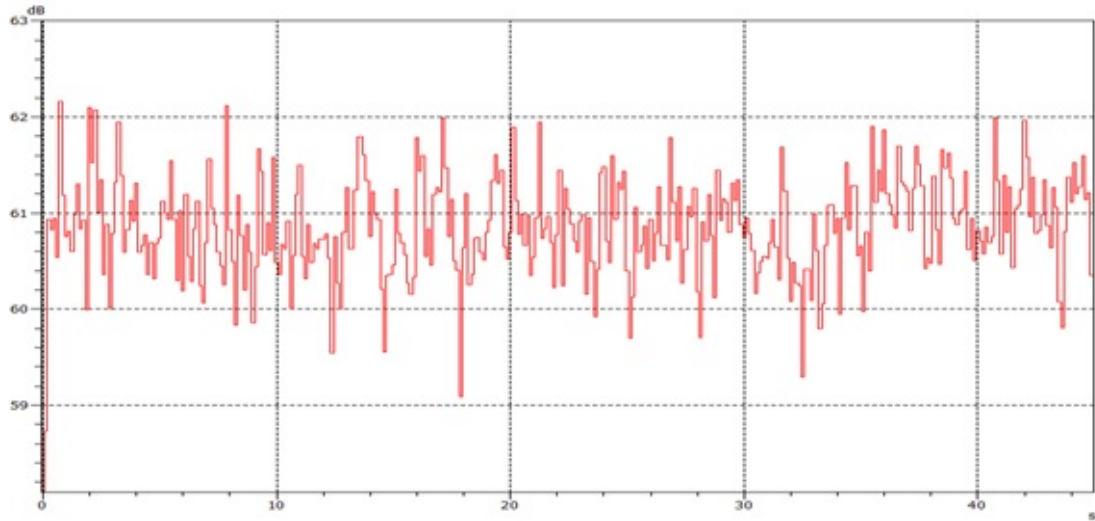
Figure 5.8: Performance feedback controller

### 5.3.4. FEEDFORWARD CONTROL: MEASURING DISTURBANCES

In this subsection disturbances will be measured and accounted for to improve performance in terms of precision. The electrical signal flowing into the loudspeakers is third octave band filtered and amplified Gaussian white noise. Although the white noise has a certain power spectral density on average, the amount of energy in a short sample of the signal varies. When the white noise is analysed by a third octave filter, this variation increases most significantly in the lower third octaves as there are fewer oscillations in the fixed time window. The fluctuations in the 1000 Hz third octave band found in our study are shown in Fig 11. The maximum deviation from the mean value is about 1.5 dB.

In the plant model the signals have a constant power spectral density. Therefore the difference between the actual (instantaneous) signal power and the model signal power can be seen as a disturbance on the plant and taken into account by feedforward control. The amount of energy in the drive signal is measured and amplified such that every fixed time block  $\Delta t$  contains the same amount of energy. This compensation is added to the feedback controller found in subsection 5.3.3<sup>2</sup> The two controllers operate in series. As

<sup>2</sup>The feedback controller is a slightly more aggressively tuned I-controller, to make sure, to make sure that po-



## 5

Figure 5.9: Energy fluctuation in 1000 Hz third octave band

a result, the controller output is the product of the feedforward controller output and the feedback controller output. In figure 5.10 both controllers are covered by the block 'Controller'.

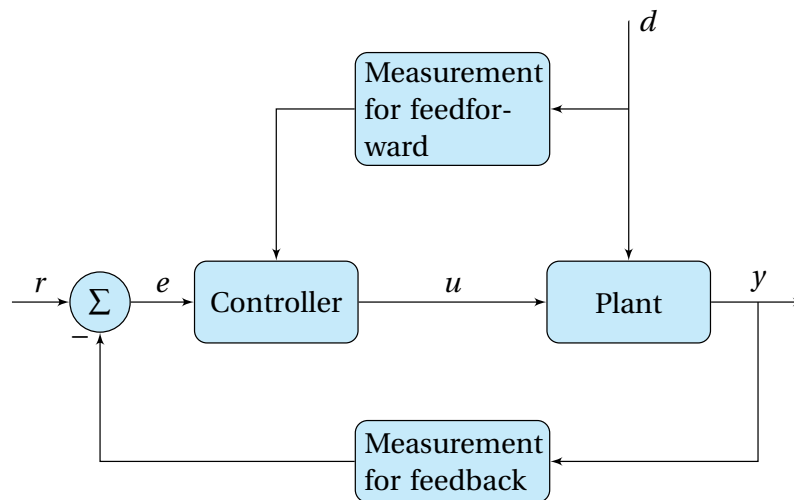


Figure 5.10: Combined feedforward- and feedback control scheme

## RESULTS

The feedforward control improved the performance considerably as can be seen in figure 5.11. The precision is smaller than 0.4 dB with approximately zero error. The signal

tential improvements are not only due to renewed feedbackcontroller, the I-controller was also applied without disturbance measurement. The results can be found in appendix A. Here it is shown that the I-controller does not outperform the PI-controller in a pure feedback control scheme.

being more stable in steady state, allows a faster feedback controller to be used. As a consequence, the start up time is slightly shorter. Since the controllers work in series,

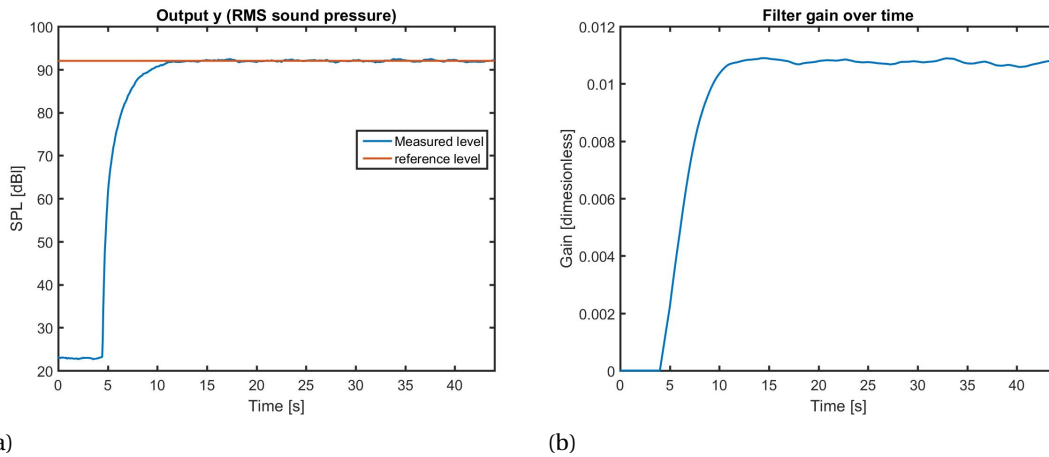


Figure 5.11: Performance after addition of disturbance measurements

their gains can be shown separately. The feedback controller gain is applied on the drive signal with an approximately constant energy level. The feedback controller gain is stable in steady state, whereas the feedforward output varies rapidly over time throughout the whole test. As the controller compensates the continuous variation of the stochastic excitation signal, the controller output was indeed expected to be a stochastic signal as well. Note that the energy in the signal is corrected at a frequency of 64 Hz. Hence, the timeblocks have a duration of:  $\Delta t = \frac{1}{64}$

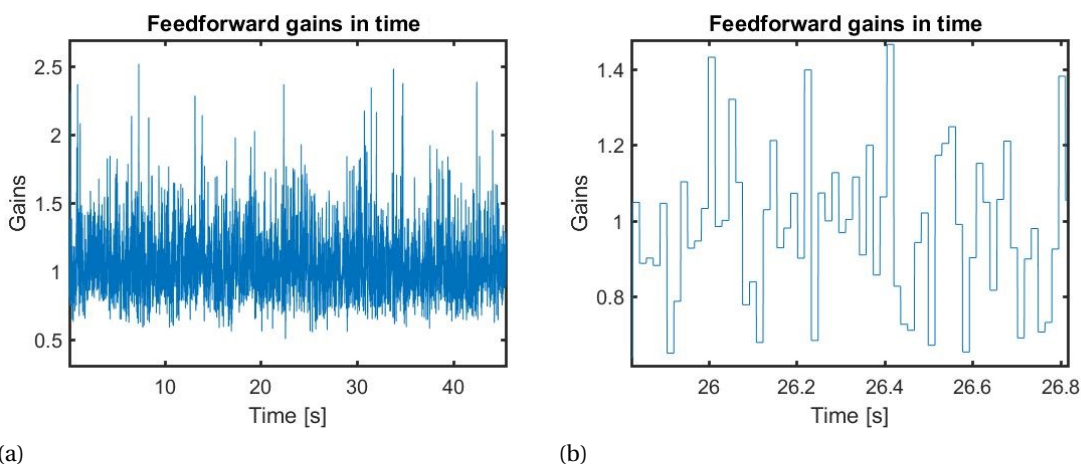


Figure 5.12: Disturbance compensation gains (linear scale)

### 5.3.5. FEEDFORWARD CONTROL: STEADY STATE INVERSE MODEL

The controller of the previous subsection performs well in terms of precision but still has a long rise-time. This is inherent to the feedback controller, when overshoot is not allowed. This subsection therefore introduces the open loop controller from subsection 5.3.2 in feedforward fashion to improve rise time. figure 5.13 shows the resulting control scheme. Notice that it also includes the previous feedforward controller and the feedback controller found in the previous section.

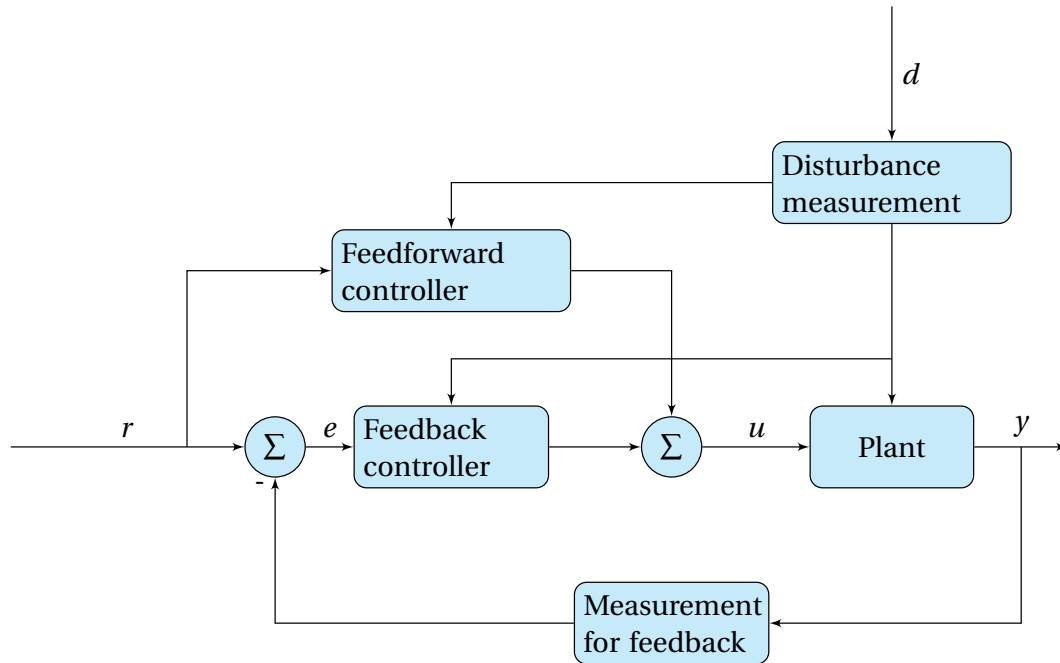


Figure 5.13: Combined feedforward- and feedback control scheme

At the test start the feedforward controller output immediately steps up to the estimated (final) gains. As such, the feedback controller only needs to compensate for the (small) error caused by the feedforward inaccuracy.

#### RESULTS

The sound pressure and gain<sup>3</sup> are shown in figure 5.14. In steady state the results are equivalent to those of subsection 5.3.4. The filter gain starts close to its steady state value at test start immediately due to the added feedforward controller. The feedback controller thereafter reduces the remaining error. Overall the steady state sound pressure level is reached much faster. This can be seen in figure 5.15. The start-up time is reduced from approximately 7 to 2 seconds.

### 5.3.6. FEEDFORWARD CONTROL: ELEVATED INITIAL GAINS

In the previous subsection the feedforward controller was the inverse model in steady state. As a result the start up time of the test was approximately equal to the rise time of the plant step response.

<sup>3</sup>Note that this again after the disturbance compensation has taken place

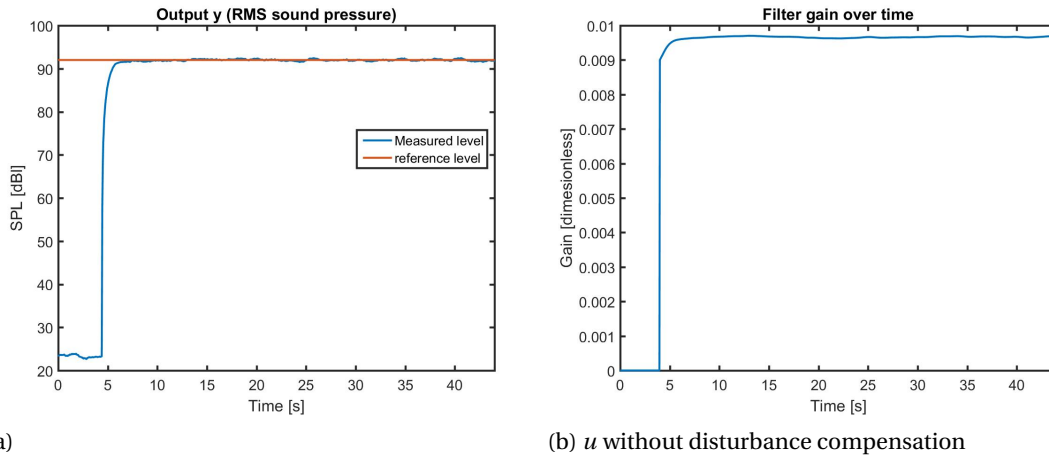


Figure 5.14: Performance

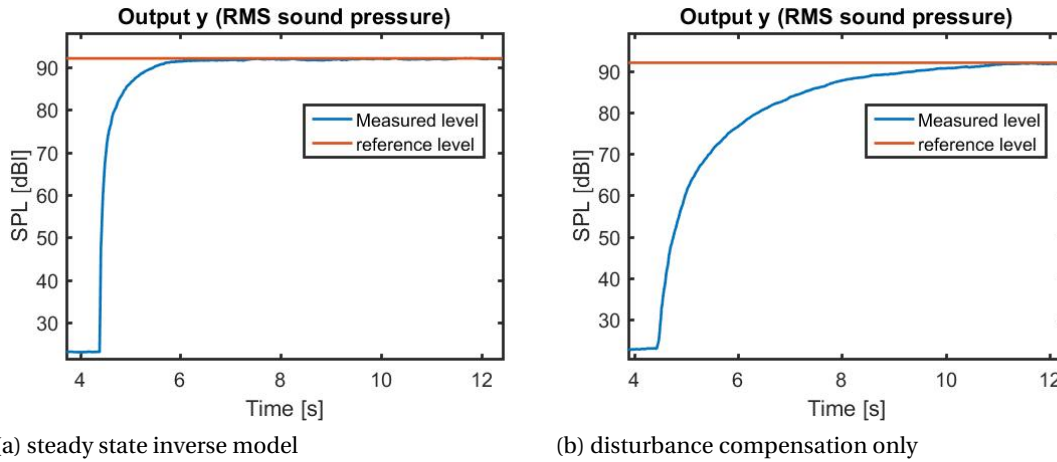


Figure 5.15: Transient behaviour output

### TRANSIENT RESPONSE

Since we are interested in the transient response, the transfer function of equation 5.1 is considered to derive the system response to the feedforward controller output  $u(s)$ . The feedforward controller output depends on the product reference signal  $r$  and the feedforward controller,  $K^{-1}$  in this case. When the test is started the controller output is immediately at this value, as such the signal is a step function. The response can be found by multiplying the system transfer function with the controller output:

$$y(s) = H(s)u(s) = \frac{K}{s\tau + 1} \frac{r}{Ks} \quad (5.4)$$

Partial fraction expansions and transformation to the time domain yields:

$$y(t) = r - r e^{-\frac{t}{\tau}} \quad (5.5)$$

The steady state output ( $t \rightarrow \infty$ ) is indeed the reference level  $r$ . To describe the expected transient behaviour the rise time is defined as the amount of time required for the response to go from 10% of its final value to 90% of its final value. Substituting these values in equation 5.5 yields an expression for the rise time:

$$t_r = \tau(\ln 0.9 - \ln 0.1) \quad (5.6)$$

Note that the rise time is not dependent on the reference level. It only depends on the systems time constant  $\tau$ , which is defined in equation 5.1. In other words, the feedforward controller will always take the same amount of time to reach a target sound pressure level, no matter what level is selected.

#### ELEVATED INITIAL GAINS

In order to decrease the test start up time even below the rise time of the room, the noise generators should shortly produce a (somewhat) higher sound power than the steady state sound power. This can be achieved by manipulating the reference signal in the control scheme of the previous subsection. When the control algorithm is initialized, the reference signal is increased with 20% for a fixed period of time  $T_{1.2}$ . From equations 5.5 and 5.5 the sound pressure level after this period of increased sound power can be found:

$$y(T_{1.2}) = 1.2r(1 - e^{-\frac{T_{1.2}}{\tau}}) \quad (5.7)$$

Rewriting yields an expression for the amount of time required to reach the reference sound pressure level:

$$T_{1.2} = \tau \ln 0.2 \quad (5.8)$$

Note that this fixed period of time is again independent of the reference level. To minimize the risk of overshoot a shorter period than computed  $T_{1.2}$  is applied.

To generalized the formula we introduce the elevation factor  $x$  (in our case 1.2). This factor can be chosen freely, provided that the direct sound field does not exceed the reference level. The elevation period then yields:

$$T_x = \tau \ln 1 - x \quad (5.9)$$

Theoretically, to reach the reference level instantly ( $T_x = 0$ ), an infinite elevation factor would be required. If one is willing to take some risk, the rise time is either limited by the maximum producible sound power or by the maximum allowable direct field sound pressure level.

#### RESULTS

In terms of steady state precision and accuracy the performance does not differ from the previous two algorithms. The start-up time has decreased, as can be seen in figure 5.17. The elevation of the reference signal has reduced the start up time from 2 to 1 second. Although this is a nice result, the principle of elevated gains is not expected to be applied. Since the benefits of a slight rise time improvement do not counterbalance the risk of overshoot inherent to this method.

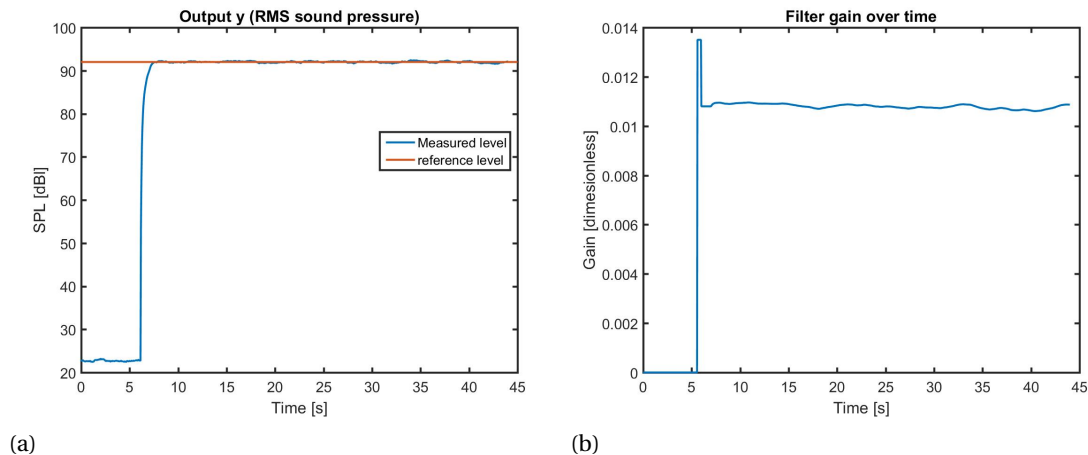


Figure 5.16: Performance elevated gains

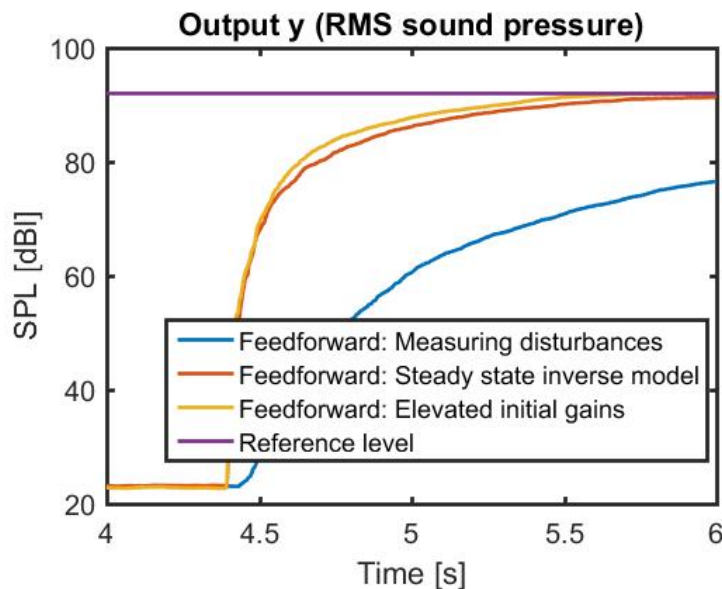


Figure 5.17: Transient behaviour

## 5.4. MULTIPLE INPUT MULTIPLE OUTPUT

The feedforward control appears to be an added value to conventional feedback control. Though, in the experiments an important simplification was applied. Only a single third octave was controlled. In this section the problem will be extended from a SISO- to a MIMO system. The control method of subsection 5.3.5 will be extended to a MIMO control method.

### 5.4.1. DECOUPLING

The goal is to control each third octave as shown in the scheme of figure 5.18 simultaneously. Writing down the relation between the inputs and output of this system yields

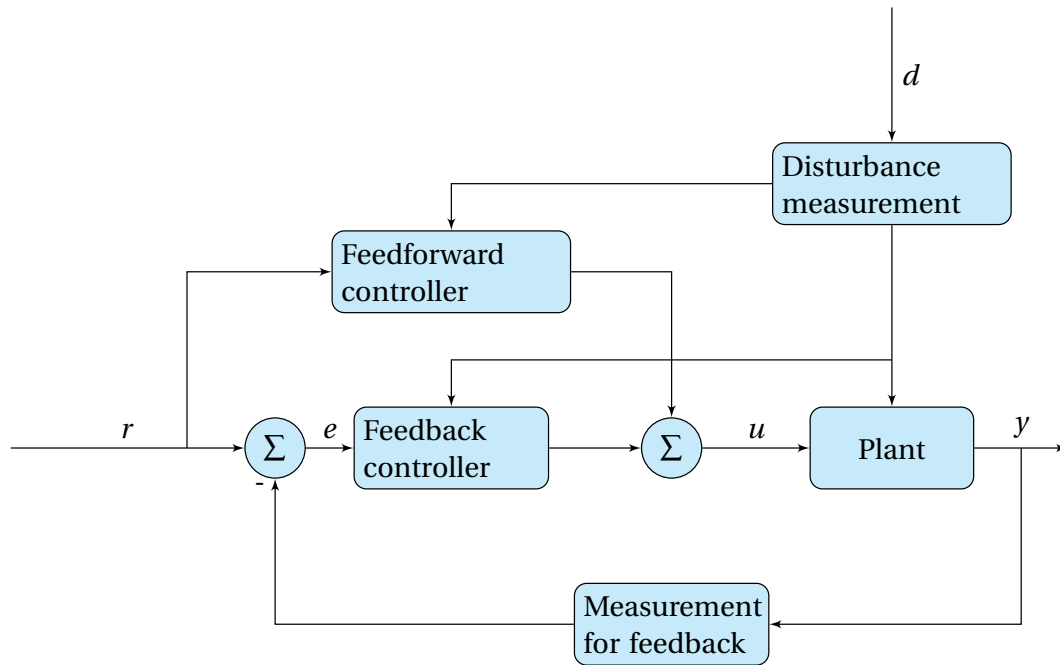


Figure 5.18: Control scheme of subsection 5.3.5

$$u = \left( \frac{k_i}{s} + k_p \right) (r - y) + \frac{r}{K} d^2 \quad (5.10)$$

Here  $k_p$  and  $k_i$  are the proportional and integral term of the feedback controller. The disturbance is defined as the factor difference between the expected energy level in the drive signal and the measured energy level in the drive signal. A reduced flow diagram of the MIMO system is shown in figure 5.19. If the diagonal entries of the operation matrix  $\mathbf{K}(s)$  now all contain the operation of equation 5.10, all third octaves are simultaneously controlled by the scheme of figure 5.18. The main challenge of the extension to MIMO

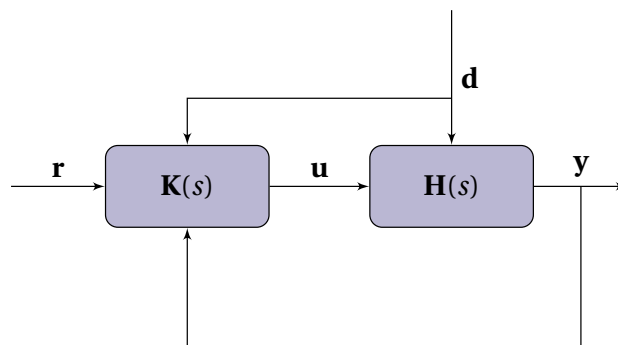


Figure 5.19: MIMO control scheme

control, is dealing with the interactions of the system. As shown in chapter 4, the interactions exist due to filtering. In consequence, control of a third octave is also observed in the measured values of adjacent third octaves. To counteract these interactions one can design a decoupling matrix  $\mathbf{X}(s)$ . In figure 5.20 the role of this decoupling matrix is

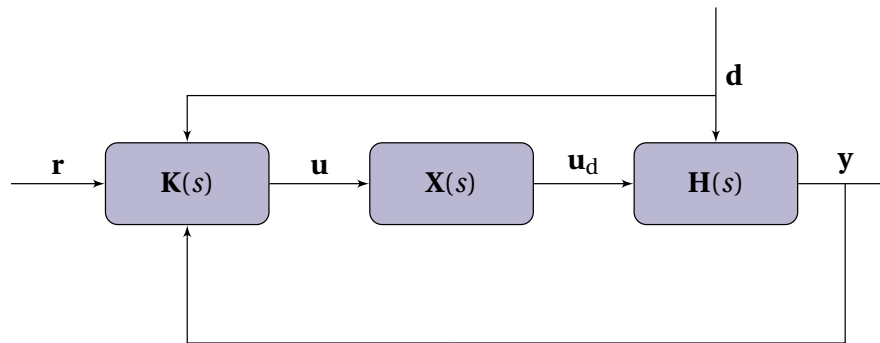


Figure 5.20: MIMO system with a decoupler

shown. The inputs  $\mathbf{u}$  are computed as if they control an individual third octave. Hence, the interactions due to filtering are not taken into account. The decoupler counteracts those interactions resulting in a shaped plant

$$\mathbf{X}(s)\mathbf{H}(s) \quad (5.11)$$

which is diagonal and easier to control. In the decoupler the interactions are compensated in advance. As a result, the decoupled inputs  $\mathbf{u}_d$  are computed. The interactions in the transfer function of the plant ( $\mathbf{H}(s)$ ) are contained in the state matrices  $\mathbf{B}$  and  $\mathbf{C}$ . The interactions are counteracted by:

$$\mathbf{X} = (\mathbf{BC})^{-1} \quad (5.12)$$

From another point of view one could say: the decoupler compensates for the filter overlap by adjusting the inputs in advance, such that after filtering the intended frequency content is fed into the acoustic noise generators

### 5.4.2. SIMULATION

The performance of the decoupler is tested in Simulink. The following third octaves were considered:

- Third octave number 1 : Centre frequency of 630 Hz
- Third octave number 2 : Centre frequency of 800 Hz
- Third octave number 3 : Centre frequency of 1000 Hz
- Third octave number 4 : Centre frequency of 1250 Hz
- Third octave number 5 : Centre frequency of 1600 Hz

It is aimed to excite the third octaves at different amplitudes. They all start at an amplitude of 500. After 25 seconds number 3 is excited to 2500. 15 seconds later its value is brought back to 1000. Furthermore number 5 is pushed up to an amplitude of 1500 after 45 seconds. Those values are the inputs  $\mathbf{u}$ . The simulation can be described in steps:

1. White Gaussian noise is generated.

2. The white noise is separately filtered by third octave bandpass filters.
3. The decoupled inputs are computed
4. The filtered signals are amplified with the corresponding  $u_d$ .
5. The five amplified signals are added, forming a single signal.
6. This signal is separately filtered by third octave bandpass filters.
7. The amount of energy per third octave is computed and is displayed as output.

Note that during a real test, between step 5 and 6, the electric energy will be transformed to acoustic energy in the acoustic noise generators and thereafter transformed back to electric energy by the microphones in the room. The amplifications in the noise generators and electric energy are assumed to be independent of frequency. Besides, the damping in the room at MBBM has a very small frequency dependence (see appendix B).

## 5

If one of these assumptions does not hold at ESA's LEAF (for example, the modulators can introduce additional non linearities.) the decoupler should be the inverse of the complete transfer function. One can then decide whether a dynamic decoupling is required or a steady state decoupling suffices.

$$\mathbf{X}(s) = \mathbf{H}(s)^{-1} \quad \text{or} \quad \mathbf{X}(0) = \mathbf{H}(0)^{-1} \quad (5.13)$$

The advantage of the latter is that it is computationally cheaper.

### RESULTS

The outputs can be seen in figure 5.21. Note that the energy level in the signals is averaged over a period of 10 seconds. This is done to avoid significant fluctuations in due to the stochastic nature of the signals. These fluctuations would hinder observing the performance of the decoupler. For comparison the same simulation is performed without the decoupler. In other words: the filtered signals are amplified with  $\mathbf{u}$  instead of  $u_d$ . Those outputs can be seen in figure 5.22. Here it can be seen that, without decoupling, the third octaves 2 and 4 are quite significantly influenced by excitation of third octave 3. Whereas the outputs after decoupling are barely affected by adjacent third octaves. Furthermore it can be seen that the excited decoupled outputs have a higher energy level during excitation. During the filtering more energy leaks from the excited third octaves to their neighbours. This phenomenon is also compensated for in the decoupler. At last there is a shortcoming of the decoupler visible as well. When the first 15 seconds of the two figures are compared, it can be observed that the five energy levels are closer to each other when the decoupler is not used. This indicates a small inaccuracy in the decoupler. However, the inaccuracy is sufficiently small to be compensated by the feedback controller.

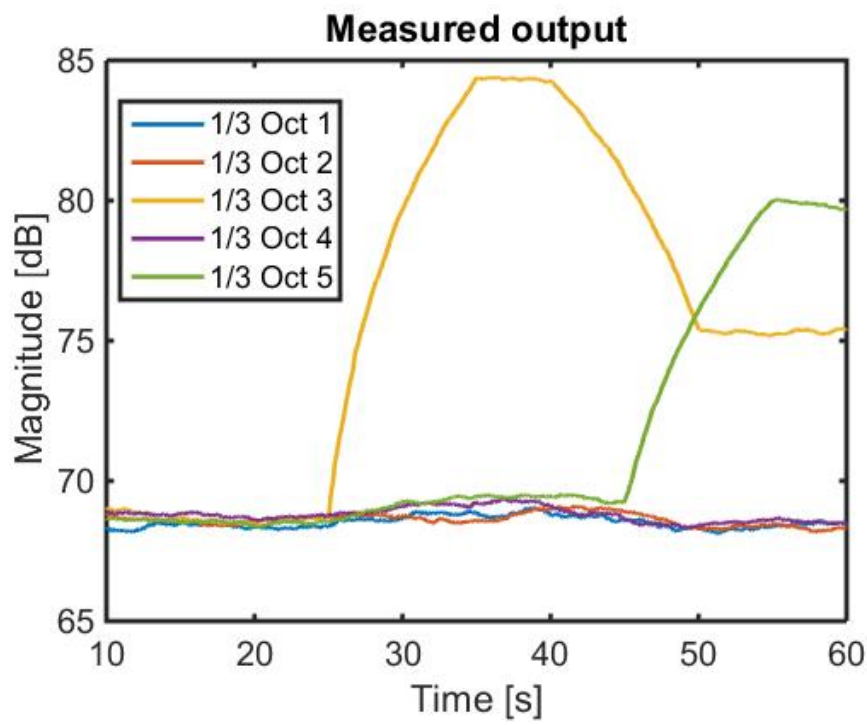


Figure 5.21: Simulation outputs with decoupler

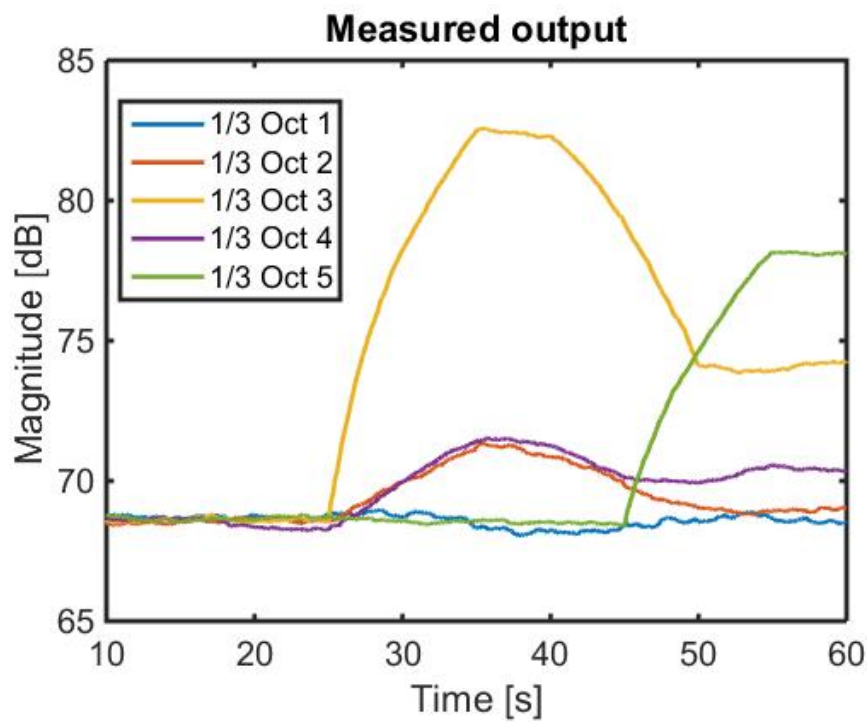


Figure 5.22: Simulation outputs without decoupler

## 5.5. SUMMARY

During a test the sound pressure level is aimed to be precise and accurate. The measure of precision in this paper is defined as the maximum absolute deviation from the mean sound pressure level in steady state. Thus in this sense, a good precision implies that the sound pressure level does not vary significantly over time. The accuracy is defined as the difference between the mean sound pressure level and the reference level in steady state. Furthermore the sound pressure levels should be approached as fast as possible. Though, the sound pressure level may not overshoot the reference level.

To meet these targets feedforward control will be used. To make a proper comparison with feedback control, the MIMO problem is reduced to a SISO problem. The performance of different control methods on the 1000 Hz third octave is tested in a small reverberation room with linear.

A steady state inverse model of the plant is the first tested controller. This controller is tested in a open loop fashion. The accuracy of this method appears to be limited. However, the steady state sound pressure level is reached in a short period of time.

From the open loop test it can be concluded that the model is not accurate enough for pure feedforward control. feedforward control can only be used in addition to feedback control. Therefore a feedback controller is designed. In comparison with the open loop control the steady state error has disappeared. This improvement is made at the expense of the short rise time. In terms of precision no progress was booked with respect to the open loop control.

To improve precision, feedforward control is added to the feedback control. The energy fluctuation in the stochastic drive signal is measured and compensated. In consequence the precision is improved.

To improve the rise time the steady state inverse model controller of the open loop control is used again. The inputs are computed, purely based on the model of the plant. The disturbances are still compensated. This approach improved the rise time.

The last method of elevated initial gains further improves the rise time. It uses the same control scheme as the previous method. However, the reference levels are increased for a short period of time. As a result the sound power will be higher in the transient time.

The performance of the different control methods are summarized in table 5.3. Here feedforward control I, II and III are the methods of measured disturbances, Steady state inverse model and the elevated initial gains respectively.

Approach	Rise time (s)	Accuracy (dB)	Precision (dB)
Open-loop control	2.5	0.8	1.1
Feedback control	10	~ 0	1.1
Feedforward control I	7.5	~ 0	0.4
Feedforward control II	2.5	~ 0	0.4
Feedforward control III	1.5	~ 0	0.4

Table 5.3: Summarized results

Taking the performance and application possibilities into account, it is chosen to extend the SISO control method of section 5.3.5 to a MIMO control method. To counteract the interactions in the plant, a decoupler is designed. First, the inputs not taking the filter overlap into account. Thereafter these inputs are corrected by the decoupler, such that the energy leakage into other third octaves is compensated. As a result, the third octaves can be controlled independently.



# 6

## CONCLUSION AND FUTURE WORK

In the final stage of this thesis alternative control approaches were evaluated. The main conclusions can be drawn from the measurements. The final product of this thesis is not yet a control algorithm, applicable on an acoustic test facility. Therefore future work is to be done.

### 6.1. CONCLUSION

Describing the sound field in the reverberation room with a model analysis loses its power as frequency increases. It is shown that the LEAF's reverberation chamber the diffuse sound field approach is justified above 150 Hz. From both the modal analysis and the diffuse sound field model acoustic energy relations can be derived. Those can be formulated in a state space representation.

With an assumed maximum overall sound pressure level of 154 dB the sound waves are still approximately symmetric around the ambient pressure of the medium. At this sound pressure level non linear propagation of the sound waves occurs. However, the resulting amount of energy leakage in other third octaves is negligible.

From the open loop test it can be concluded that the first order model captures most of the reverberation room characteristics already. Variations due to room temperature and others, do clearly show feedback control is also needed to compensate for any steady state errors though. Replacing the open loop system by a feedback controller eliminates the steady state error from open loop system. The feedback controller does not yield more precision in steady state though and also greatly compromises on rise time.

One can improve on steady state precision by adding a feedforward controller. In specific this feedforward controller should compensate for the continuous variation of the stochastic excitation signal. In our study, adding this time of feedforward improved the precision in our test from 1.1 dB to 0.4 dB.

One can furthermore improve on rise time by adding another feedforward controller. One can do so by exploiting the open loop model. As such, at test begin, instant initial gain estimates for steady state operation are set, requiring the feedback controller to only

compensate for the remaining error. In our study application of this control yielded near theoretical rise times for a reverberation room.

To reduce the rise time even further, elevated gain levels compared to the open loop model may also be used. It was shown that this approach reduces the rise time even further, i.e. in our study from 2 seconds to 1 second only. It was also shown that the rise time is independent on sound pressure level increase and may therefore be applied safely.

The interactions in the MIMO transfer function are caused by the filter overlap in the frequency domain. It has been shown that those interactions can be counteracted by a decoupler. In consequence, the system can be controlled by a purely diagonal control matrix.

Overall it can be concluded that feedforward control adds value to the conventional feedback control of acoustic testing. Measuring the power of white noise and compensating for that by means of feedforward control has shown to improve performance in terms of precision. Furthermore, feedforward control has shown to be capable of reducing the start-up time of the test significantly.

## 6.2. FUTURE WORK

The experiments in this thesis took place in a small reverberation room with linear loudspeakers. In the LEAF, for example, the sound power is generated by modulators and horns. An air/nitrogen flow is spectrally modulated ([2]) and flows through the horns into the room.

The input-output relation of the noise generation can possibly be very non linear. Consequently, the linear model of the plant, used for control does not hold any more. Furthermore, the acoustic noise generation can cause additional interactions in the transfer function.

Therefore the acoustic noise generation of a real test facility should be identified and the possible findings should be included in the model of the plant, as well as in the decoupler.

## REFERENCES

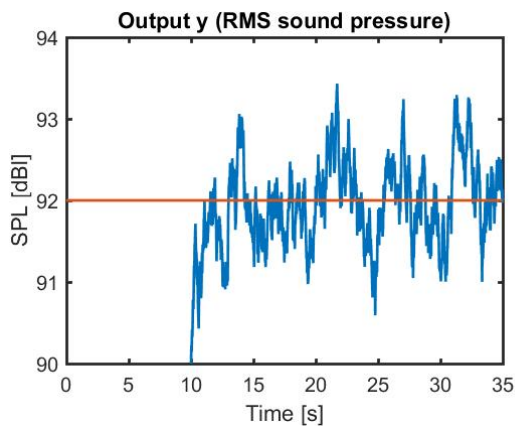
- [1] Anant Grewal: *High Intensity Noise Generation for Extremely Large Reverberant Room Test Applications* Sensors, Instrumentation and Special Topics, Volume 6.
- [2] ECSS Executive Secretariat: Space engineering, Spacecraft mechanical loads analysis handbook, ESA Requirements and Standards Division, 2013.
- [3] Finn Jacobsen: The sound field in a reverberation room, Technical University of Denmark, 2011.
- [4] Daniel J Ricksen: Mechanical Analysis for engineering, Delft University of Technology, 2011.
- [5] Carl Hopkins: *Sound Insulation* , Routledge, New York 2014.
- [6] H. Kuttruff: Sound in enclosures. Chapter 91 in *Encyclopedia of Acoustics* Wiley and Sons, New York, 1997 .
- [7] Colin Hansen: Fundamentals of acoustics, University of Adelaide.
- [8] Buye Xu: Generalized Acoustic Energy Density and Its Applications, Birmingham Young University, 2010.
- [9] James P. Chambers and Paul Jensen: Noise control. Chapter 13 in *Advanced Air and Noise Pollution Control* Volume 2, 2005
- [10] Evgenia A. Zabolotskaya: Green's functions for a volume source in an elastic half-space, The Journal of the Acoustical Society of America, 2012.
- [11] G.G. Stokes: On the theories of the internal friction in fluids in motion, *Transaction of the Cambridge Philosophical Society*, vol. 8, 1845.
- [12] Lothar Cremer and Helmut A. Muller: *Die wissenschaftlichen Grundlagen der Raumakustik*, Volume 2, Applied science publishers, London 1982.
- [13] Vincent Tournat: Introductory Lecture on non linear acoustics, Laboratoire d'"acoustique de l'Universite du Maine, 2014.
- [14] Werner Lauterborn, Thomas Kurz, Iskander Akhatov: non linear Acoustics in Fluids. Chapter 8 in *Springer handbook of acoustics*, 2014.

- 
- [15] Karl Janssens: *Closed-Loop Acoustic Control of Reverberant Room for Satellite Environmental Testing* Proceedings of the 12th European Conference on Spacecraft Structures, Materials and Environmental Testing, held 20-23 March, 2012 at ESTEC, the Netherlands
- [16] N.S. Bakhvalov, Y.M. Zhileikin, E.A. Zabolotskaya: *non linear Theory of Sound Beams*, American Institute of Physics, Melville, 1987.
- [17] S. Earnshaw: On the mathematical theory of sound, Philos. Trans. R. Soc. London, 1860
- [18] James Stewart: *Calculus Early Transcendentals*, 8th Edition, 2015.
- [19] Dilip Sarwate: *Matched Filters Part I*, University of Illinois, University of Illinois, 2011
- [20] F.M. Dekking, C. Kraaikamp, H.P. Lopuhaa, L.E. Meester: *A modern introduction to probability and statistics*. Springer, 2005.
- [21] Cleve Moler: *Cleve Moler on Mathematics and Computing*, Scientific computing, math and more.
- [22] J.S.Chitode: *Digital signal processing*, Technical Publications, 2008.
- [23] Clarence W. Da Silva: *Modeling and Control of Engineering Systems*, Taylor and Francis Group, 2009.
- [24] Sigurd Skogestad and Ian Postlethwaite: *Multivariable Feedback Control Analysis and design*, John Wiley & Sons.
- [25] J. S. Bendat, A. G. Piersol: *Random Data*, Wiley-Interscience, 1986.
- [26] Adrian S Nastase: "How to Derive the RMS Value of Pulse and Square Waveforms". *MasteringElectronicsDesign.com*. Retrieved 21 January 2015.

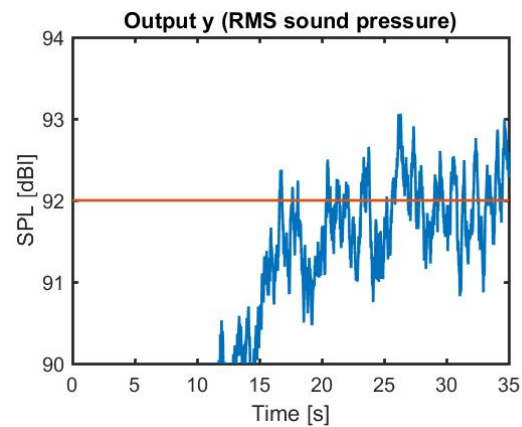
# A

## PI vs I IN FEEDBACK CONTROL

In figure A.1 the output of two measurements is displayed. Here to different feedback controllers are tested in a pure feedback control scheme. The I controller is the feedback controller of subsection 5.3.4 and the PI controller is the one from subsection 5.3.3. As can be seen the PI controller has a slightly better precision. This comparison is made to confirm that the improved precision of the control method in subsection 5.3.4 can be assigned to the disturbance compensation, rather than the renewed feedback controller.



(a) I



(b) PI

Figure A.1: Pure feedback performance: I vs PI



# B

## REVERBERATION TIMES

Third octave centre frequency (Hz)	Reverberation time (s)
50	4.65
63	4.22
80	4.71
100	4.64
125	4.97
160	5.09
200	5.52
250	5.13
315	4.99
400	5.19
500	5.27
630	5.09
800	4.94
1000	5.11
1250	5.28
1600	5.29
2000	4.88
2500	4.29

Table B.1: Reverberation times, reverberation room at MBBM. These values are experimentally determined as described in ISO 354.